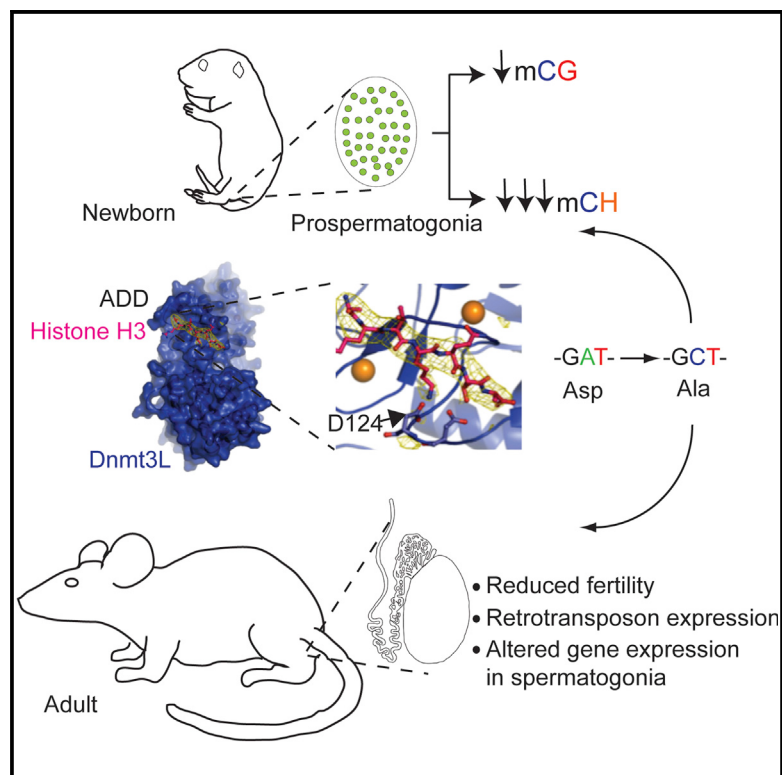


The Dnmt3L ADD Domain Controls Cytosine Methylation Establishment during Spermatogenesis

Graphical Abstract



Authors

Georgios Vlachogiannis,
Chad E. Niederhuth, ..., Robert J. Schmitz,
Steen K.T. Ooi

Correspondence

s.ooi@ucl.ac.uk

In Brief

The adaptor protein Dnmt3L plays a crucial role in establishing cytosine methylation during male gametogenesis, but its mechanism of action is unclear. Vlachogiannis et al. now show that the N-terminal ADD domain is necessary for full methylation establishment, with CH sites being critically dependent on this domain.

Highlights

- Full establishment of CG methylation during male gametogenesis requires Dnmt3L ADD
- Non-CG methylation establishment critically requires Dnmt3L ADD
- Correct spermatogenesis and fertility requires Dnmt3L ADD
- Defects are a consequence of altered gene expression and retroelements expression

Accession Numbers

GSE58066



The Dnmt3L ADD Domain Controls Cytosine Methylation Establishment during Spermatogenesis

Georgios Vlachogiannis,¹ Chad E. Niederhuth,² Salih Tuna,¹ Athanasia Stathopoulou,¹ Keijo Viiri,^{1,4} Dirk G. de Rooij,³ Richard G. Jenner,¹ Robert J. Schmitz,² and Steen K.T. Ooi^{1,*}

¹Epigenetic Signaling Group, Department of Cancer Biology, UCL Cancer Institute, Paul O'Gorman Building, 72 Huntley Street, London WC1E 6BT, UK

²Department of Genetics, University of Georgia, 120 East Green Street, Athens, GA 30602, USA

³Center for Reproductive Medicine, Academic Medical Center, University of Amsterdam, 1105 AZ Amsterdam, the Netherlands

⁴Present address: Paediatric Research Centre, University of Tampere Medical School and Tampere University Hospital, 33520 Tampere, Finland

*Correspondence: s.ooi@ucl.ac.uk

<http://dx.doi.org/10.1016/j.celrep.2015.01.021>

This is an open access article under the CC BY license (<http://creativecommons.org/licenses/by/4.0/>).

SUMMARY

A critical aspect of mammalian gametogenesis is the reprogramming of genomic DNA methylation. The catalytically inactive adaptor Dnmt3L is essential to ensuring this occurs correctly, but the mechanism by which it functions is unclear. Using gene targeting to engineer a single-amino-acid mutation, we show that the Dnmt3L histone H3 binding domain (ADD) is necessary for spermatogenesis. Genome-wide single-base-resolution DNA methylome analysis of mutant germ cells revealed overall reductions in CG methylation at repetitive sequences and non-promoter CpG islands. Strikingly, we also observe an even more severe loss of non-CG methylation, suggesting an unexpected role for the ADD in this process. These epigenetic deficiencies were coupled with defects in spermatogonia, with mutant cells displaying marked changes in gene expression and reactivation of retrotransposons. Our results demonstrate that the Dnmt3L ADD is necessary for Dnmt3L function and full reproductive fitness.

INTRODUCTION

Cytosine methylation is a key chromatin modification required for normal gene regulation and genome stability (Goll and Bestor, 2005). In mammals, it is predominantly found in CG dinucleotides, functioning in the silencing of retrotransposons and regulation of single-copy sequences and genes subject to parent-of-origin imprinting. While rare in most tissues and differentiated cells, methylome analysis reveals that non-CG methylation is abundant in embryonic stem cells (ESCs) (Lister et al., 2009), germ cells (Kobayashi et al., 2013), and the brain (Lister et al., 2013; Xie et al., 2012), although its function remains unclear. DNA methylation is established during gametogenesis, following erasure in sexually uncommitted primordial germ cells (PGCs) (Seisenberger et al., 2012). In males, PGCs entering the gonadal

ridge differentiate into prospermatogonia (PSG)/gonocytes that are mitotically arrested by 16.5 days postcoitum (dpc) (Vergouwen et al., 1991). Between 16.5 dpc and 2 days postpartum (dpp), genome-wide de novo DNA methylation is thought to be restored to prior levels, ensuring the correct resetting of DNA methylation imprints. Following birth, prospermatogonial stem cells (PSCs) re-enter the cell cycle (Clermont and Perey, 1957), migrate to and colonize the seminiferous tubule basement membranes, and establish the initial pool of spermatogonial stem cells (SSCs) that maintain spermatogenesis for the rest of the animal's life (Kluin and de Rooij, 1981; Yoshida et al., 2006).

DNA methylation is established by two DNA methyltransferases, Dnmt3A and Dnmt3B (Okano et al., 1999). In addition, a catalytically inactive adaptor, Dnmt3L, is essential for this process to occur properly during gametogenesis (Bourc'his and Bestor, 2004; Bourc'his et al., 2001; Hata et al., 2002; Webster et al., 2005). *Dnmt3L*-deficient male animals are azoospermic due to a block in meiosis at the leptotene-zygote transition, marked by non-homologous synapsis/meiotic catastrophe. Retrotransposons are reactivated due to a failure to establish methylation at these elements. Furthermore, although initially present, SSCs are reportedly depleted by 8–10 weeks of age, resulting in mutant testes containing seminiferous tubules completely devoid of germ cells (Hata et al., 2006).

Given the critical role of Dnmt3L in gametogenesis, much attention has centered on understanding the mechanism by which it operates. Biochemical assays indicate Dnmt3L directly associates with both Dnmt3A and Dnmt3B; crystallographic studies using the C-terminal domains of murine Dnmt3A and Dnmt3L indicate this interaction is mediated through the C-terminal methyltransferase folds (Jia et al., 2007). Dnmt3L functions as an allosteric activator (Chedin et al., 2002; Suetake et al., 2004) and improves Dnmt3A processivity (Holz-Schietinger and Reich, 2010). DNMT3L forms heterotetrameric complexes with DNMT3A (Jia et al., 2007), forming filaments coating DNA molecules in vitro (Jurkowska et al., 2008). *Dnmt3L* encodes a ~50-kDa protein and contains an N-terminal cysteine-rich ATRX-Dnmt3-Dnmt3L (ADD) domain (Aapola et al., 2002). Using either human or mouse Dnmt3L proteins, we and others have shown that the ADD domain interacts with the N terminus of

histone H3. Importantly, this in vitro interaction can be disrupted by an aspartic acid to alanine mutation at position 90 or 124 in human or mouse Dnmt3L protein, respectively (Hu et al., 2009; Ooi et al., 2007; Otani et al., 2009; Zhang et al., 2010). This observation has given rise to the Dnmt3L histone recognition hypothesis (Ooi et al., 2010), whereby the recognition of DNA methylation target sequences is dependent on the ability of Dnmt3L to bind to histone H3.

As mentioned, existing studies into Dnmt3L biological function have relied on null alleles that completely eliminate expression of Dnmt3L protein. Although greatly informative, this approach prevents a direct test of whether or not the ADD is involved in Dnmt3L function. In addition, given that Dnmt3L functions in complex with Dnmt3A/Dnmt3B, it is unclear the degree to which the phenotypes observed are a direct consequence of disrupting Dnmt3L protein or other proteins dependent on Dnmt3L expression/presence. Using a “knockin” approach, we have generated a mouse strain with a single-amino-acid mutation to test the biological importance of the ADD domain.

RESULTS

Defective Cytosine Methylation, Particularly at Non-CG Contexts, in *Dnmt3L^{A/A}* Prospermatogonia

In agreement with our previous biochemical studies on human DNMT3L, we observed that mouse Dnmt3L protein binds to histone H3 and that a D124A mutation within the Dnmt3L ADD is sufficient to disrupt this binding (Figure 1A). To test the biological importance of this residue, the D124A mutation (hereafter referred to as *Dnmt3L^A*) was introduced into the endogenous *Dnmt3L* locus by homologous recombination in ESCs and animals were generated by subsequent breeding (Figures S1A–S1D). *Dnmt3L^{A/A}* animals were viable, consistent with the *Dnmt3L^{-/-}* phenotype. To examine the extent of methylation defects in *Dnmt3L^{A/A}* germ cells, we performed whole-genome bisulphite sequencing (WGBS) on fluorescence-activated cell sorting (FACS)-purified PSG from 1-day-postpartum (1-dpp) wild-type and mutant animals. Germ cells were purified by combining the D124 mutation with a germ cell reporter transgene (*Oct4-GiP*), which expresses GFP under the control of the *Oct4* promoter (Ying et al., 2002).

Analysis of the sequence context of cytosines identified as being methylated in 9.85×10^8 mapped reads revealed that as well as canonical CG methylation, wild-type PSG harbored significant numbers of reads containing methylated cytosines in a non-CG context (Figure 1B). It is well known that most cytosines in a CG context in mammals are typically methylated and undergo deamination to TpG, which results in CG dinucleotides representing a much smaller than expected proportion of total cytosines. Indeed, in our dataset, mapped reads containing CG dinucleotides (irrespective of methylation state) constitute only 3.86% of the total (Table 1). We found that 72% of cytosines that showed evidence of methylation occur in a non-CG context; this is in line with that previously published in embryonic day 16.5 (E16.5) PSG (Kobayashi et al., 2013), which have not yet completed de novo methylation, as well as in growing oocytes (Shirane et al., 2013) (49% and 66%, respectively). Consistent with this, analysis of the level of non-CG methylation from bisulphite PCR data at long inter-

spersed nuclear element-1 (LINE-1) and intracisternal A particle (IAP) elements also supports these findings of abundant non-CG methylation (Figure S1E). Motif analysis revealed that most non-CG methylation occurs at TNCAG and TNCAC motifs (Figure 1C), consistent with previous observations in germ cells (Kobayashi et al., 2013, Shirane et al., 2013), human ESCs (Lister et al., 2009), and brain (Lister et al., 2013).

We next examined the effects of the D124A mutation on cytosine methylation. Globally, numbers of methylated CG sites in *Dnmt3L^{A/A}* PSG relative to that observed in wild-type were reduced (Figure 1D). Analysis of the methylation level throughout the genome divided into 100-bp bins indicated CG methylation was significantly reduced in *Dnmt3L^{A/A}* PSG compared to wild-type (Wilcoxon rank sum test, $p < 2.2 \times 10^{-16}$) (Figure 1E). To determine if any specific compartment was affected, we compared weighted methylation levels within various genomic compartments. The majority of CG dinucleotides are located within the repetitive compartment of the genome. Analysis of CG methylation at LINEs, long terminal repeats (LTRs), and short interspersed nuclear elements revealed that while these elements were predominantly methylated in wild-type germ cells, these were hypomethylated in *Dnmt3L^{A/A}* mutant cells (Figures 1F and S1F). This is consistent with both methylation-sensitive Southern blot and bisulphite sequencing data examining LINE1 and IAP sequences showing elements that are both normally methylated and hypomethylated (Figures S1G and S1H). Analysis of CpG islands (CGIs) revealed differences depending on context. As expected, those associated with gene promoters were largely unmethylated in both wild-type and mutant cells (Figure 1F). CGIs not associated with promoters (so-called orphan CGIs; Illingworth et al., 2010) tended to be methylated, with reductions in mutant cells. As well as repetitive elements, DNA methylation is also established at paternally imprinted differentially methylated regions (DMRs). CG methylation at paternally imprinted loci trended toward reduced levels in *Dnmt3L^{A/A}* germ cells (Figure 1G), with significant reductions at the Gpr1/Zdbf2 and Rasgrf1 DMRs (Fisher exact test values, 6.66×10^{-4} and 4.73×10^{-5} , respectively). Interestingly, the Rasgrf1 DMR, which is associated with an adjacent repetitive region, showed the greatest reduction (49% versus 19% methylation). As expected, analysis of maternally imprinted DMRs revealed these to be hypomethylated. These data indicate that despite Dnmt3L protein being present, full establishment of CG methylation at repeats and the paternally imprinted DMRs analyzed is defective in *Dnmt3L^{A/A}* germ cells.

In addition to the global reduction in CG methylation, we also observed a drastic reduction in non-CG methylation in *Dnmt3L^{A/A}* PSG relative to wild-type (Figures 1D and 1E). We note that the level of expression of components of the Dnmt3 complex was not significantly altered by the D124A mutation (Figure S1I), arguing that the observed methylation defects could not be attributed to reduction in the expression levels of these proteins. Analysis of non-CG methylation in various genomic compartments revealed that similar to CG methylation, this was reduced throughout all regions in *Dnmt3L^{A/A}* PSG, with most non-CG methylation found in non-promoter-associated CGIs (Figures 1F and S1F). Together, these data suggest that non-CG methylation is crucially dependent on correct ADD function.

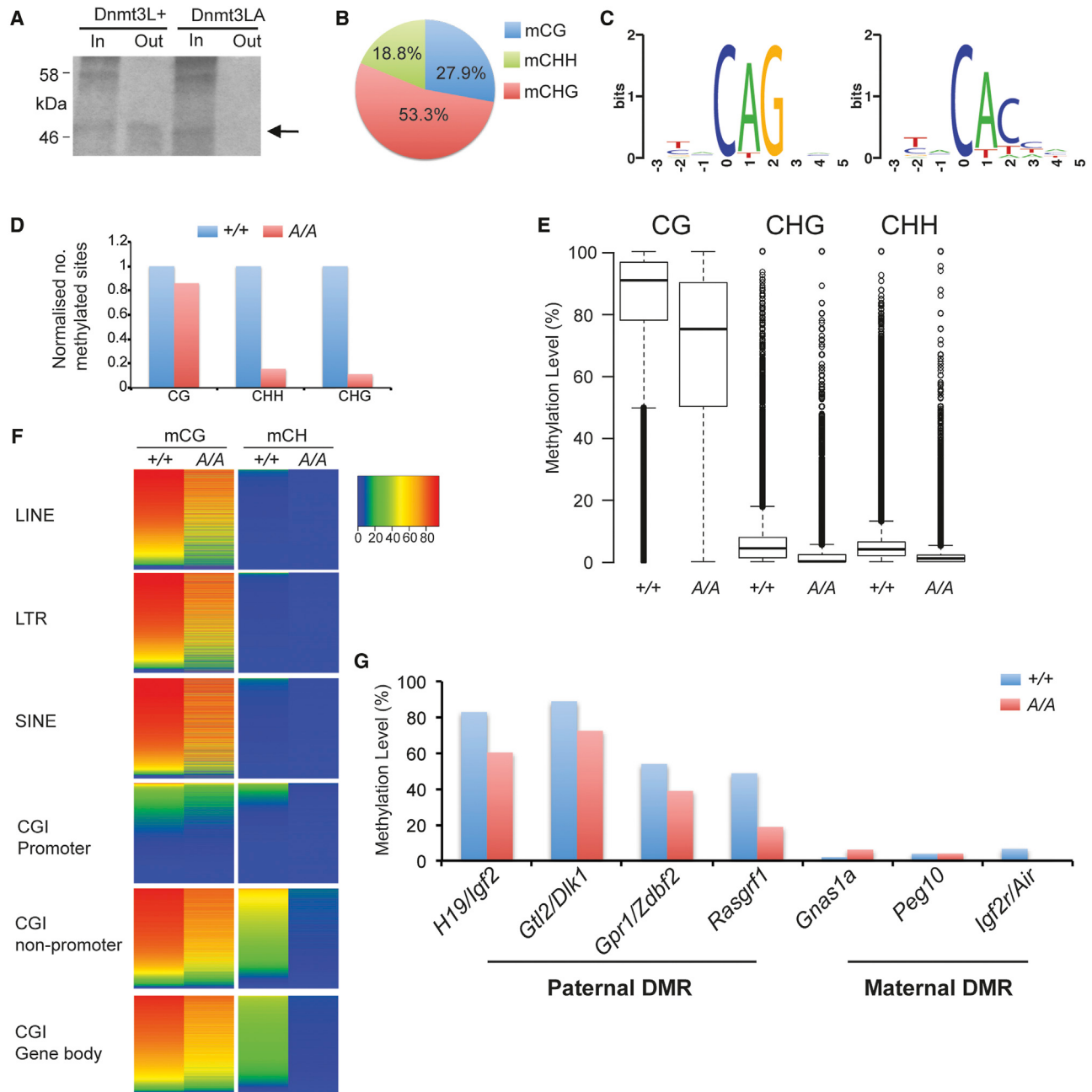


Figure 1. Whole-Genome Bisulphite Sequence Analysis in Prospermatogonia

(A) Peptide pull-down data showing interaction between in vitro transcribed and translated recombinant mouse Dnmt3L protein and the N terminus of histone H3 peptide (amino acids 1–21). Arrow indicates Dnmt3L protein. Higher bands in input lanes represent BSA, used as a blocking agent during peptide binding. Proteins were resolved on a 7.5% polyacrylamide gel and subsequently stained using Bio-Safe Coomassie stain (Bio-Rad). Note that this interaction is specifically lost upon mutation of aspartic acid into alanine at position 124 (D124A).

(B) Pie chart showing distribution of methyl cytosine in CG, CHG, and CHH contexts in wild-type prospermatozoa (PSG). Only uniquely mapped reads were used in this and subsequent analyses. H refers to any base except a guanine.

(C) WebLogo plots for bases proximal and distal to methylated cytosines in CHG and CHH contexts.

(D) Bar graphs comparing relative normalized numbers of methylated sites in wild-type versus *Dnmt3L*^{A/A} PSG.

(E) Box-whisker plots showing methylation levels throughout wild-type and *Dnmt3L*^{A/A} PSG genomic DNA divided in 100-bp bins. Boxes represent quartiles and whiskers demarcate maximum and minimum values. Exact p value is $< 2.12 \times 10^{-16}$.

(F) Heatmaps indicating levels of CG methylation at different sequence classes indicated.

(G) Bar graphs depicting methylation levels at paternal and maternal imprinted differentially methylated regions (DMRs). DMR coordinates were obtained from Xie et al. (2012).

Table 1. Number of Mapped Reads Containing Methylated and Unmethylated Cytosines in Different Sequence Contexts in *Dnmt3L*^{+/+} and *Dnmt3L*^{A/A} 1-dpp Prospermatogonia

	Methylated		Unmethylated		Total	
	<i>Dnmt3L</i> ^{+/+}	<i>Dnmt3L</i> ^{A/A}	<i>Dnmt3L</i> ^{+/+}	<i>Dnmt3L</i> ^{A/A}	<i>Dnmt3L</i> ^{+/+}	<i>Dnmt3L</i> ^{A/A}
CG	3.03×10^7	2.54×10^7	7.76×10^6	1.17×10^7	3.81×10^7	3.71×10^7
CHH	5.79×10^7	8.8×10^6	6.68×10^8	7.02×10^8	7.26×10^8	7.10×10^8
CHG	2.04×10^7	2.24×10^6	1.86×10^8	2.01×10^8	2.06×10^8	2.03×10^8
Total	1.09×10^8	3.64×10^7	8.61×10^8	9.14×10^8	9.70×10^8	7.26×10^8

Dnmt3L ADD Ensures Hypermethylation at Normally Methylated Loci in Prospermatogonia

CG methylation outside of promoter regions but within gene bodies has been reported to show a positive correlation with the level of transcription (Hellman and Chess, 2007). We therefore considered whether such an association existed in PSG. Using available RNA-sequencing data, we examined CG methylation at genes highly expressed in E16.5 PSG (Seisenberger et al., 2012). Contrary to published data, average levels of both CG and non-CG methylation within highly expressed genes showed slight but significant reductions compared to levels observed at weakly expressed genes (Figure 2A). We note also that average methylation levels of both these sets of genes are lower still compared to that observed within the bodies of all RefSeq genes. This argues that, at least in PSG, there is no direct positive correlation between the levels of CG methylation within genes and transcriptional activity.

Consistent with this, we observe that both CG and CH methylation across the bodies of genes in several groups closely track that observed along all RefSeq genes (Figure 2B). In other words, gene-body methylation is observed across all genes and it is generally reduced in *Dnmt3L*^{A/A} germ cells. Our data indicate that full methylation across gene bodies is dependent on Dnmt3L function. In addition, when we compare gene-body CG methylation of all mouse RefSeq genes in wild-type 1-dpp PSGs with that observed in other tissues, we find substantially higher levels of methylation (Figure 2C). In line with all other compartments analyzed, CG gene-body methylation at all RefSeq genes was significantly reduced in *Dnmt3L*^{A/A} PSG compared to wild-type (Figure 2D). Genome-wide analysis of the distribution of CG methylation levels indicates that relative to other tissue types, PSG are hypermethylated, which is attenuated in *Dnmt3L*^{A/A} germ cells (Figure 2E).

Dnmt3L^{A/A} Male Animals Have Defective Spermatogenesis and Reduced Fertility

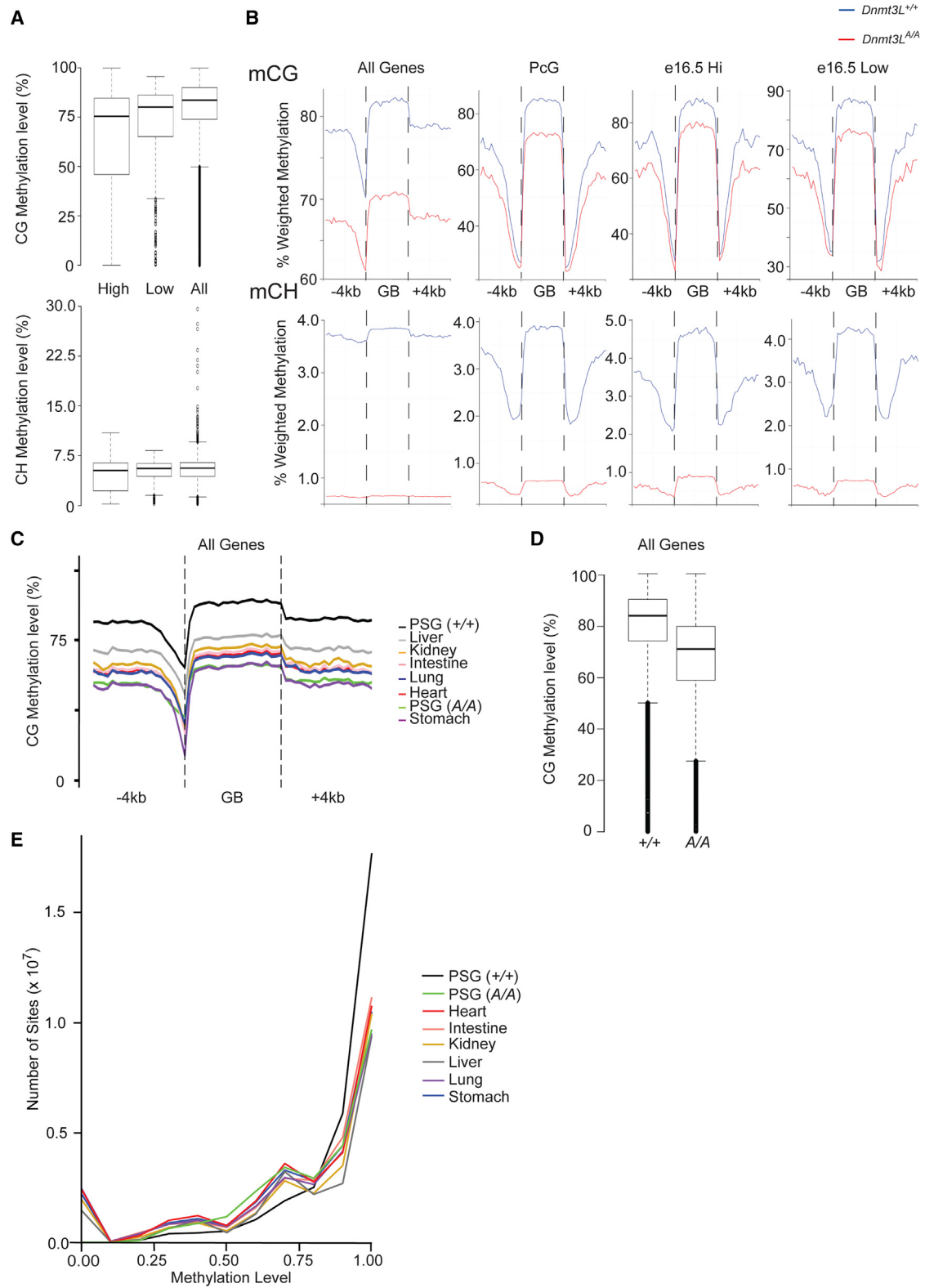
We next sought to determine the effects of the *D124A* mutation on testes development and fertility. Analysis of *Dnmt3L*^{A/A} stud males revealed that although they were capable of siring offspring, they were subfertile, with significant reductions in overall testes size (Figure 3A) and various metrics of reproduction (Figure 3B). In a few cases, animals were found to be completely azoospermic. Histological examination of mutant testes unexpectedly revealed the presence of seminiferous tubules devoid of germ cells beyond the spermatocyte stage, co-existing with tubules displaying all stages of spermatogenesis (Figure 3C, see panels I and II). Staging analysis revealed

apoptosis of large cohorts of spermatocytes in some tubules in stage IV while no apoptosis of spermatocytes was observed in other stage IV tubules (Figures S2A–S2F). When apoptosis occurred, round and elongating spermatids were also absent in the affected area. These observations suggest that *Dnmt3L*^{A/A} spermatocytes have a diminished chance to survive the stage IV checkpoint. However, spermatocytes can survive stage IV and continue to develop normally through to mature spermatozoa. This explains the phenotype of tubules with normal, complete spermatogenesis, adjacent to tubules lacking generations of spermatocytes and spermatids. We note that spermatogonia and, depending on the epithelial stage, early types of spermatocytes were always present at 12.5 to 16 weeks of age (Figures S2A–S2F). This developmental block is consistent with previously published data showing that seminiferous tubules in *Dnmt3L*-deficient testes do not progress beyond stage IV (Webster et al., 2005). The proportion of defective tubules in different *Dnmt3L*^{A/A} animals varied, with some animals being significantly affected while others showed minimal signs of defective tubules (Table 2). FACS analysis on germ cells from mutant animals carrying the *Oct4-GFP* transgene showed that *Dnmt3L*^{A/A} male animals had significant reductions in absolute numbers of GFP⁺ cells, which translated to reductions at all spermatogenic stages (Figures 3D, S2G, and S2H). Analysis of meiotic spreads revealed the presence of both homologous (normal) as well as non-homologous (abnormal) synapsis events (Figure 3E). Taken together, these data indicate that the *D124A* mutation is hypomorphic and that the ADD is necessary for normal Dnmt3L biological activity.

D124A Mutation Disrupts Gene Expression in SSCs

The SSC niche is maintained by a delicate balance of signals promoting either self-renewal or differentiation. Previously published data examining *Dnmt3L* null animals showed that spermatogonia are completely absent by 8–10 weeks of birth, caused by stem cell exhaustion (Hata et al., 2006). As mentioned above, despite the presence of defective tubules, histological analysis indicated that germ cells were present beyond 8–10 weeks of birth. Histological analyses of testes from 1-dpp animals suggested the absence of any reduction in the numbers of PSG that initially seed the seminiferous tubules (Figures S2I and S2J). This is consistent with previous reports showing no difference in numbers of PSG in *Dnmt3L*-deficient animals (Hata et al., 2006).

To better understand the mechanisms by which the *D124A* mutation causes spermatogenic defects, we examined the transcriptional consequences in FACS-purified spermatogonia.



(legend on next page)

Cells were purified from 9-dpp animals to examine the immediate consequences of the *D124A* mutation in newly differentiating spermatogonia and to assist purification of sufficient numbers of cells for analysis. Microarray analysis revealed up- and downregulation of 530 genes and 411 genes, respectively in *Dnmt3L^{A/A}* SSCs (Figure 4A). Among other processes, Gene Ontology (GO) analysis revealed a reduction in the expression of genes involved in cell fate commitment as well as those containing homeobox domains (Figures 4B and S3). qRT-PCR for markers of undifferentiated spermatogonia and genes functionally important in SSCs maintenance and differentiation revealed reductions in the expression of various markers/transcriptional regulators, including significant reductions in *Pou5f1/Oct4*, *Sox3*, *Dazl*, *Ngn3*, and *Sohlh2* (Figure 4C) (Phillips et al., 2010).

Consistent with functions in development, we found that genes downregulated in *Dnmt3L^{A/A}* SSCs are enriched for polycomb target genes. Metagene analysis of ESC chromatin immunoprecipitation sequencing (ChIP-seq) data revealed an enrichment of the polycomb repressive complex 2 (PRC2) subunit Suz12 at genes downregulated in *Dnmt3L^{A/A}* SSCs (Figure 5A). Similarly, using lists of PRC2 target genes in ESCs (Ku et al., 2008), we found that while 10% of all genes are associated with PRC2, this increases to 36% for genes that are downregulated in *Dnmt3L^{A/A}* spermatogonia; upregulated genes showed only an 8% overlap with Suz12 binding. Downregulated genes are therefore 3.5 times more likely to be a target for the PRC2 complex. A similar enrichment was observed when examining both a second PRC2 component (Ezh2) as well as the post-translational histone modification it mediates (H3K27me3) (Figures 5B and 5C), with 44% of downregulated genes associated with the modification compared to 29% for upregulated genes (27% of all genes are associated with this modification). We note that in 1-dpp PSG, both CG and non-CG methylation profiles across gene bodies of Pcg target genes are very similar to methylation profiles of non-expressed and all RefSeq genes (Figure 5D), arguing against a direct interaction between Dnmt3L-targeted methylation and the regulation of these genes. These data suggest that de-regulation of genes involved in spermatogenesis and development contribute to the observed defects in germ cell function.

Retrotransposons Are Activated by the *D124A* Mutation

We next sought to provide insights into the potential mechanisms by which the *D124A* mutation might affect gene induction. The 5' regulatory regions of retrotransposons, particularly IAP

and LINE1 elements, are known targets for CG methylation and can possess enhancer activity (Schmidt et al., 2012). In situ hybridization using probes for these elements revealed that *Dnmt3L^{A/A}* mutant testes display a mosaic pattern of expression, with some tubules showing high levels of expression and other tubules showing little or no expression (Figures 6A and 6B). Interestingly, this is consistent with our histological data indicating defects in some, but not all, seminiferous tubules. Consistent with this, analysis of our microarray data of 9-dpp spermatogonia indicated that transcripts containing retrotransposons were also upregulated in *Dnmt3L^{A/A}* animals (Figure 6C). We then examined whether there was any relationship between the de-regulated genes we observed in *Dnmt3L^{A/A}* spermatogonia and their proximity to mapped repetitive elements. Proximity analysis revealed that on average, upregulated genes tended to be closer to the endogenous retrovirus (ERV) class of retroelements, which include IAP elements (Figure 6D; exact p values are 0.01279 [upregulated genes] and 0.9953 [downregulated genes]). Analysis of the methylation state in 1-dpp PSGs of ERVs represented on the array indicated that these too were hypomethylated in *Dnmt3L^{A/A}* compared to wild-type germ cells (Figures 6E and 6F). This supports a model whereby the Dnmt3L ADD functions to ensure full methylation and silencing of these elements, in turn necessary to prevent ectopic gene expression during spermatogenesis.

DISCUSSION

The mechanism by which epigenetic information is both established and maintained is of great importance but remains poorly defined, particularly interactions between different epigenetic processes. The adaptor Dnmt3L is crucial for the establishment of DNA methylation during gametogenesis. However, previous data in the literature were obtained using genetic models lacking expression of Dnmt3L, and little is known about which of the domains present in Dnmt3L is required for regulation of epigenetic reprogramming during gametogenesis. We have now shown that the ADD is necessary for correct Dnmt3L biological function, potentially through its ability to control non-CG methylation and CG methylation and repression of retrotransposons.

To the best of our knowledge, our results are the first demonstration of the importance of the Dnmt3L ADD in gametogenesis. Our own data and that of others have shown that in vitro, the *D124A* mutation results in loss of histone H3 binding. A recent study reported that the Dnmt3L ADD directly interacts with the

Figure 2. CG and Non-CG Methylation Is Observed at Similar Levels across All Genes and Reduced by *D124A* Mutation

- (A) Box-whisker plots of normalized CG and CH methylation levels across genes highly and weakly/not expressed in E16.5 PSG. Methylation levels at all RefSeq genes are also shown. E16.5 PSG expression data were obtained from Seisenberger et al. (2012). Wilcoxon rank sum test results comparing highly to weakly expressed genes were 1.403×10^{-5} and 4.091×10^{-4} for CG and CH methylation, respectively.
- (B) Metaplots showing gene-body methylation at CG and CH in the various gene groups indicated. Blue and red lines denote levels observed in wild-type and mutant, respectively. Note that levels are similar irrespective of gene activity.
- (C) Metaplot of normalized CG methylation levels across all genes in the different cell types and tissues indicated.
- (D) Box-whisker plots showing CG methylation levels within all RefSeq genes in wild-type and *Dnmt3L^{A/A}* PSG. Result of Wilcoxon rank sum test, E16.5 high versus E16.5 low: $p = 1.403 \times 10^{-5}$ (mCG), $p = 4.091 \times 10^{-4}$ (mCH).
- (E) Graph showing the distribution of methylation levels of each methylated cytosine in the genome in the different tissues and cell types indicated. The shift to the right (closer to 1.0 or 100%) indicates that many more methylcytosines are methylated 100% of the time based on the sequencing data compared to lower individual methylation levels observed in germ cells. The frequency of methylated cytosines methylated at the highest levels is greater in wild-type than *Dnmt3L^{A/A}* germ cells and other somatic tissues tested. The data indicate that PSG are hypermethylated compared to differentiated tissues.

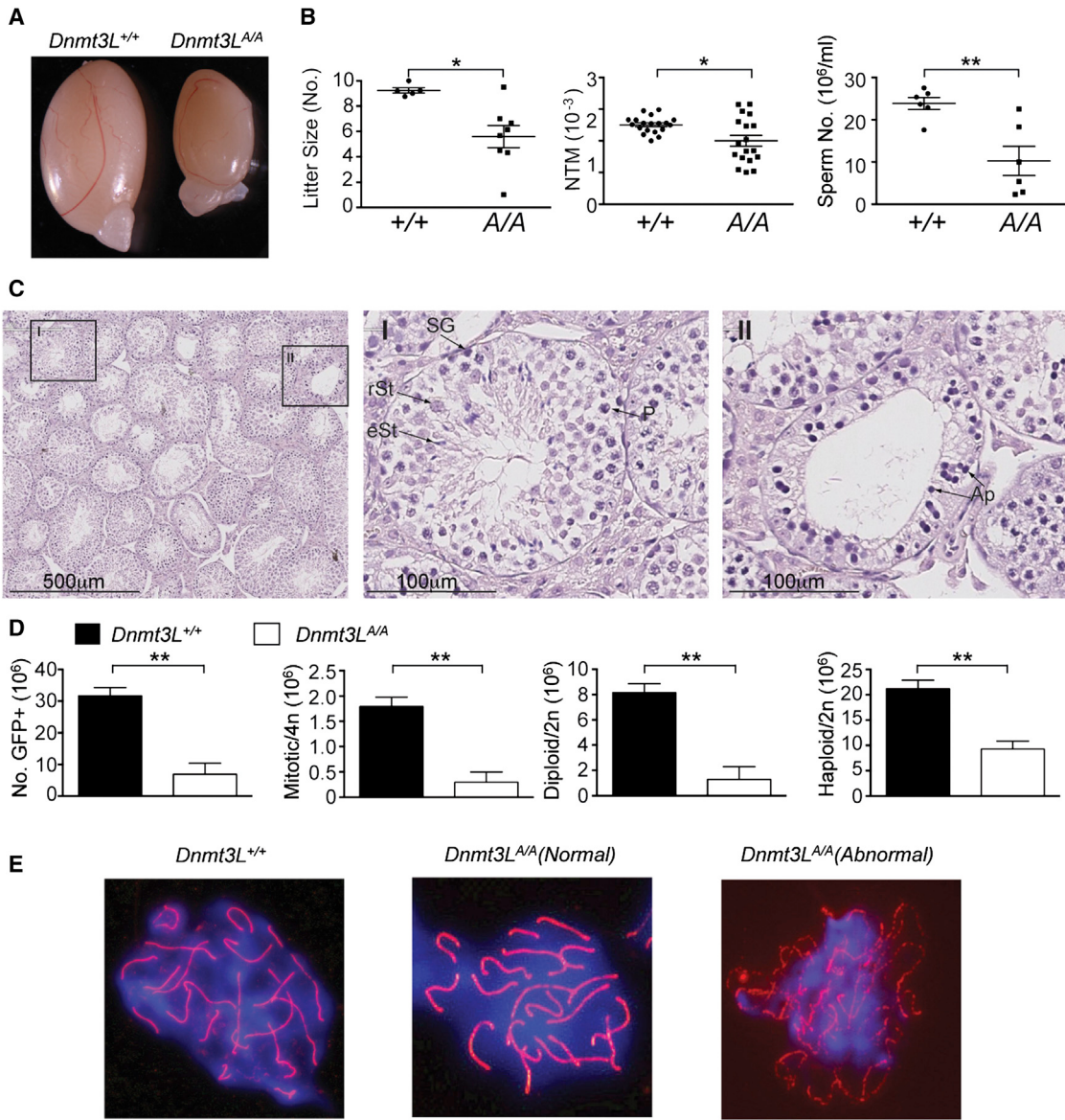


Figure 3. Dnmt3L D124A Mutation Causes Fertility Defects

(A) Image of testes removed from 15-week-old *Dnmt3L^{+/+}* and *Dnmt3L^{A/A}* animals.

(B) Biometric data comparing *Dnmt3L^{+/+}* and *Dnmt3L^{A/A}* animals. Note that *Dnmt3L^{A/A}* animals have a significant reduction in testes mass (*Dnmt3L^{+/+}*: n = 19, age: 8–19 weeks; *Dnmt3L^{A/A}*: n = 18, age: 8–19 weeks). *Dnmt3L^{A/A}* males also produce significantly less spermatozoa than age-matched *Dnmt3L^{+/+}* males (n = 6, age: 15–17 weeks). Two *Dnmt3L^{A/A}* animals were found to be azoospermic. The average litter sizes sired by *Dnmt3L^{A/A}* stud males were also reduced (5.6 pups versus 9.2 pups). For *Dnmt3L^{+/+}* animals, four litters from four different studs were recorded. For *Dnmt3L^{A/A}* animals, eight different litters from eight different studs were recorded. Scatterplots show mean ± SEM. Exact p values are 0.0374 (normalized testes mass, NMT), 0.0087 (sperm counts), and 0.0283 (litter sizes).

(C) Low- (6×) and high-magnification (30×) images of H&E-stained sections of fixed and paraffin-embedded testes from a *Dnmt3L^{A/A}* male (16 weeks). Note the coincidence of normal (I) and empty (II) seminiferous tubules. SG, spermatogonia; P, pachytene spermatocyte; rSt, round spermatid; eSt, elongating spermatid; Ap, apoptotic cell.

(D) Bar graphs depict absolute cell numbers (mean ± SEM) of the different cell populations indicated measured by FACS. Exact p values are 0.0059 (GFP⁺) and 0.0012 (mitotic/4n, diploid/2n, and haploid).

(E) Immunofluorescence micrographs of meiotic spreads from either *Dnmt3L^{+/+}* or *Dnmt3L^{A/A}* testes. Spreads were stained using Scp1 (synaptonemal complex 1) antibody. Note that *Dnmt3L^{A/A}* males produce spermatocytes capable of undergoing correct chromosomal pairing (normal) as well as spermatocytes defective in the process (abnormal).

PRC2 component Ezh2 in ESCs (Neri et al., 2013). In contrast, our own studies have failed to detect interaction between endogenous Dnmt3L and Ezh2 by co-immunoprecipitation using an

anti-Dnmt3L antibody (Figure S4). As it is unknown whether the D124A mutation would similarly affect Ezh2 interaction, and given the extensive literature demonstrating ADD interaction

Table 2. Analysis of the Frequency of Defective Tubules in Testes Sections from *Dnmt3L*^{+/+} and *Dnmt3L*^{A/A} Animals

Genotype	Age (Weeks)	Number	
		Normal	Defective
<i>Dnmt3L</i> ^{+/+}	17	200	0
<i>Dnmt3L</i> ^{A/A}	18	140	9
<i>Dnmt3L</i> ^{A/A}	16	95	73
<i>Dnmt3L</i> ^{A/A}	18	175	58
<i>Dnmt3L</i> ^{A/A}	15	0	200

In each transverse section, 200 tubules were counted.

with histone H3, we favor the interpretation that the phenotypes reported in this study are a consequence of defective histone H3 binding and chromatin association.

Our results indicate that the *D124A* mutation is a hypomorphic allele; male *Dnmt3L*^{A/A} animals are subfertile with reductions in various metrics of fertility, which is somewhat unexpected. Based on the histone recognition model, abrogation of histone H3 binding should result in a failure by Dnmt3L to correctly recruit Dnmt3A/B methyltransferases to all methylation target loci. Therefore, one would predict that *Dnmt3L*^{A/A} male animals should phenocopy *Dnmt3L*^{-/-} animals (complete sterility instead of subfertility). The animals used in the studies reported carry the *D124A* mutation on an outbred background, which might account for the incomplete penetrance of the reported phenotype. We have found that combining the *D124A* mutation with a null allele (*Dnmt3L*^{A/-}) resulted in male animals that were all azoospermic, had microchidia, and whose testes only contained tubules with defective spermatogenesis (Figure S5). Combined with our observations in *Dnmt3L*^{A/A} animals, this supports a dosage effect and that despite the presence of one copy of Dnmt3L, the *D124A* mutation has critical consequences on gametogenesis and phenocopies complete absence of Dnmt3L protein.

Our analyses of the transcriptional defects observed in *Dnmt3*^{A/A} undifferentiated spermatogonia provide insight into the spermatogenesis phenotypes previously observed in *Dnmt3L*-deficient animals. Our bioinformatics analyses support the notion that retrotransposons can serve as aberrant controlling elements to enhance the expression of nearby genes. They also underscore the importance of correct expression of developmental regulators and genes involved in stem cell maintenance. Although a recent study has implicated Dnmt3L protein in playing a direct functional role in SSCs (Liao et al., 2014), our results and those of others do not corroborate this finding. It has previously been reported that Dnmt3L protein is no longer expressed from 2 dpp (Sakai et al., 2004), although there is evidence for the presence of Dnmt3L mRNA that cannot be translated (O'Doherty et al., 2011). We have been unable to detect the presence of Dnmt3L protein in FACS-purified spermatogonia (Figure S6), which leads us to conclude that the transcriptional defects we observe at this stage of spermatogenic development are a consequence of perturbations during the preceding PSG stage.

Given the general importance of Dnmt3L in establishing methylation at cytosines, our finding that non-CG methylation is substantially affected by the *D124A* mutation is striking and

unexpected. It is widely considered that as both CG and non-CG methylation is dependent on the Dnmt3 de novo machinery, any perturbation in Dnmt3L function would be predicted to affect both types of methylation equally. As both CG and non-CG methylation are completely obliterated in *Dnmt3L* null animals, our results suggest differences in the mechanism by which methylation is established in CG and non-CG contexts, namely that the latter is greatly dependent on the Dnmt3L ADD domain.

Genomic non-CG methylation has been described in pluripotent stem cells (Lister et al., 2009), germ cells (both growing oocytes and PSG; Shirane et al., 2013; Kobayashi et al., 2013), and prefrontal cortical neurons (Lister et al., 2013). Common features of these cell types are the expression of Dnmt3A and the fact that they are non-cycling. Dnmt3L protein expression has not been documented outside of pluripotent and germ cells; consistent with this, we failed to detect Dnmt3L in prefrontal cortex from juvenile male animals (Figure S6B). The absence of detectable levels of Dnmt3L combined with our observation that germ cells are dependent on Dnmt3L-histone H3 binding for non-CG methylation suggests cell-type-specific mechanisms in how this modification may be regulated.

It has long been known in mammals that CG methylation is predominantly located in repetitive elements and imprinted DMRs. Our results show that Dnmt3L-histone association plays a general role to ensure that these sequences are methylated to the correct levels. We note that not all paternally imprinted loci are equally affected by the *D124A* mutation. The most severely affected DMR, *Rasgrf1*, is considered to be an atypical paternally imprinted locus with a DMR associated with an adjacent tandem repetitive region (Shibata et al., 1998). Our results also add to the debate over the function of gene-body methylation. We observed a general reduction across these regions in *Dnmt3L*^{A/A} PSG, consistent with reductions in CG methylation in retroelements that are predominantly located in introns. However, our results suggest that at least in PSG, there is no conspicuous association with highly as compared to weakly/non-expressed genes; this argues that if there is any correlation, it is subtle. This is similar to the observation in hESCs, which show higher overall CG methylation compared to somatic cells and the existence of partially methylated domains (Lister et al., 2009). We propose that positive associations between transcription levels and gene-body methylation may vary in a cell-type-dependent manner.

Our results imply that the genomes of germ cells such as PSG may have the highest overall levels of DNA methylation of all mammalian cell types described which we propose is a consequence of Dnmt3L expression. This leads to the prediction that cell types expressing Dnmt3L should have high levels of CG methylation. In accordance with this, we note that hESCs, which also express Dnmt3L, have been reported to have high levels of CG methylation (Lister et al., 2009).

Expression of Dnmt3L renders PSG hypermethylated relative to genomes of other tissues, and our results show this to be a default process necessary for full reproductive fitness. An outstanding question is how genomic regions remain refractory to cytosine methylation, specifically promoter-associated CGIs and maternally imprinted DMRs. We propose that future studies

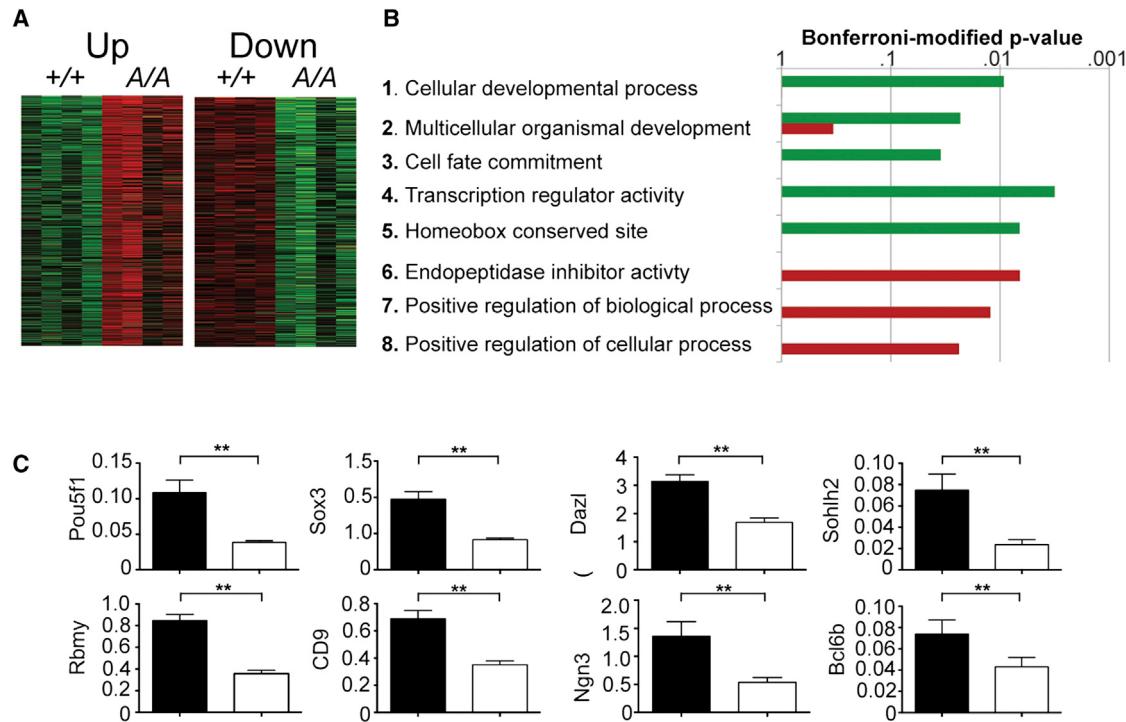


Figure 4. Altered Gene Expression in *Dnmt3L*^{AA} Spermatogonia

(A) Heatmap of median-normalized genes showing more than a 2-fold \log_2 difference in expression. Rank product analysis revealed the upregulation and downregulation of 530 and 411 genes, respectively, in *Dnmt3L*^{AA} (A/A) versus wild-type (+/+) germ cells. SSCs were FACS-purified from four individual 9-dpp animals of each genotype.

(B) Bonferroni-modified p values for the enrichment of selected representative functional gene categories in the sets of genes upregulated or downregulated in *Dnmt3L*^{AA} SSCs. Categories 1–3, 7, and 8 are Gene Ontology biological processes, 4 and 6 are Gene Ontology molecular functions, and 6 is an Interpro domain. No Interpro domains were enriched in the set of upregulated genes.

(C) qRT-PCR analysis of SSC markers. Bar graphs show mean \pm SEM. Exact p values are 0.0022 (Pouf51, Sox3, Dazl, Rbmy, CD9), 0.0087 (Ngn3, Sohlh2), and 0.0455 (Bcl6b).

should focus on defining the pathways and mechanisms that specifically prevent or interfere with Dnmt3L-histone H3 interaction. Pertinent to this are in vitro data showing that methylation of H3K4 disrupts DNMT3L-histone H3 peptide binding (Ooi et al., 2007) and recent genome-wide observations showing dynamic changes in H3K4Me2 immediately preceding the timing of de novo methylation (Singh et al., 2013). Such studies will provide a more comprehensive understanding of the interaction between different epigenetic processes and their biological roles.

EXPERIMENTAL PROCEDURES

Probes for Retrotransposons

IAPs were detected using the probe described previously (Michaud et al., 1994). The probe is derived from the IAP element responsible for the *A^{iap}* allele and recognizes the LTR. For LINE-1 detection, a probe derived from the 5' UTR of a truncated L1Md-A3.6 element (GenBank accession number M13002) was used. Primer sequences used were as follows: IAP-14A (5'-NNNNNGGGCC CGCAGAGAAGGTGATCGGTGG-3'), IAP-13K (5'NNNNNGGTACCTGTTATT GACGCCTTCTCA-3'), L1Md-A2F (5'-CCCAACATAGAGTCCTGA-3'), and L1Md-A2R (5'-AGTGGGCAGAGTATTCTC-3').

In Situ Hybridization

Experiments were performed as described previously (Bourc'his and Bestor 2004).

Antibodies

For *in situ* hybridization, incorporated digoxigenin (DIG) was detected using alkaline-phosphatase-conjugated anti-DIG Fab fragments (Roche Diagnostics). For immunofluorescence, anti-Scp1 rabbit polyclonal (ab15090, Abcam) was used. For chromatin immunoprecipitation, the following antibodies were used: anti-Suz12 (ab12073, Abcam), anti-H3K27me3 (ab6002, Abcam), and anti-H3 (ab1791, Abcam).

Purification of Germ Cells and Preparation of Nucleic Acids

Undifferentiated spermatogonia from 9-dpp males were purified using the method described previously (Garcia and Hofmann, 2012). Note this method was also used to prepare testicular germ cells for FACS analysis. For 1-dpp testes, male animals were sacrificed and pairs of testes removed. Tubules were dissociated by collagenase. Single-cell suspensions were prepared by incubation with Accutase (Sigma) and passing through a cell strainer. Germ cells were purified on either a FACSAria III or Mo-Flo cell sorter, with purities for both wild-type and mutant germ cells at >98%. DNA was prepared using the QIAamp Micro Kit (QIAGEN), and RNA was prepared using the High Pure RNA Isolation Kit (Roche). All animals used for this study were covered by a Home Office Project License under The Animals (Scientific Procedures) Act 1986 to S.K.T.O. This research study was also approved by the UCL Research Ethics Committee. Animals were humanely sacrificed at a designated establishment by cervical dislocation.

Meiotic Spreads

Meiotic spread were prepared according to the method described previously (Peters et al., 1997).

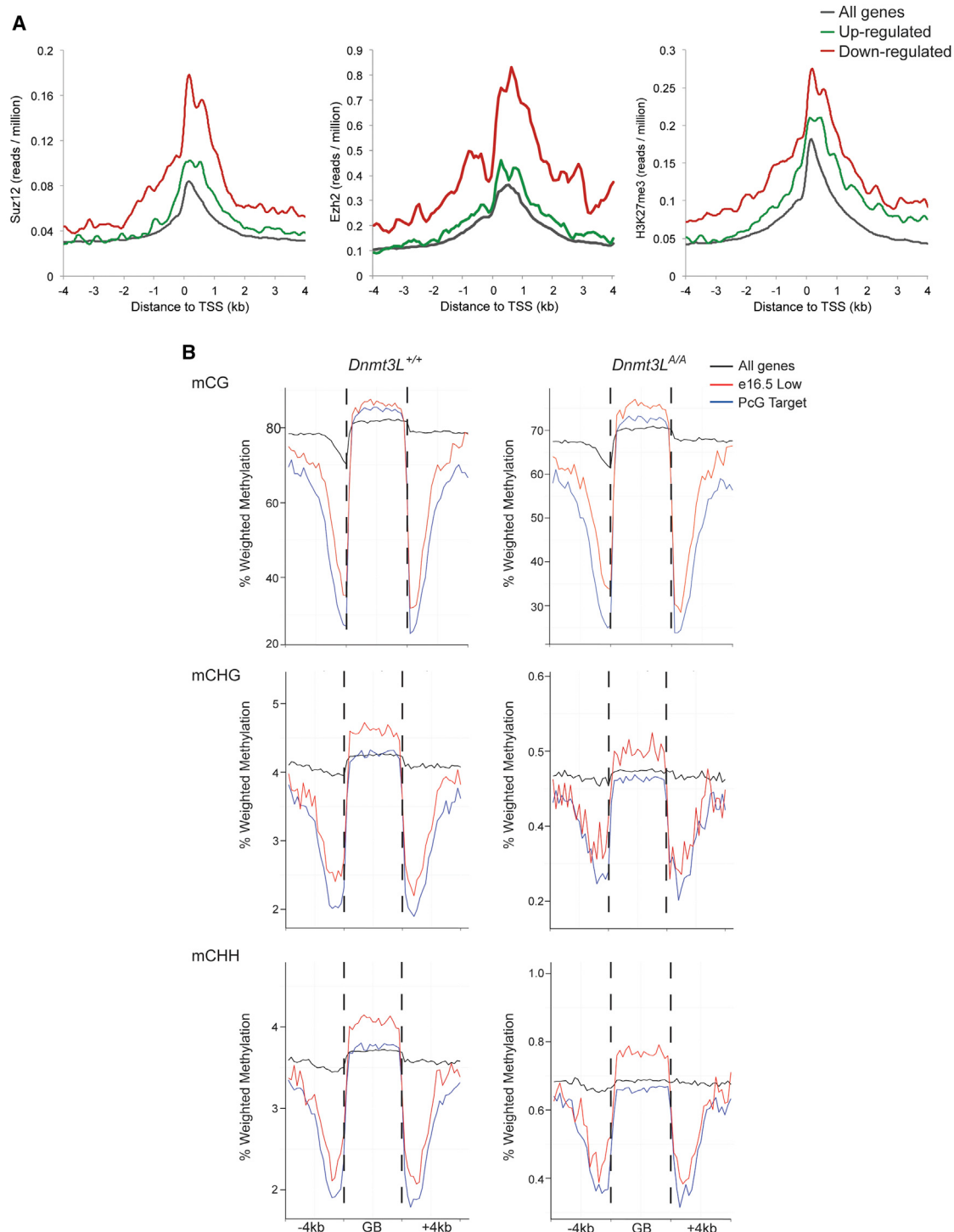


Figure 5. PRC2 Components and H3K27Me3 Are Enriched at Genes Downregulated in *Dnmt3L*^{A/A} SSCs

(A) Metagene plot of *Suz12*, *Ezh2*, and *H3K27Me3* along the gene body (± 4 kb of the transcription start site [TSS]) showing downregulated genes are more likely to be targets of the PRC2 complex. Plots show the average number of ChIP-seq sequence reads for *Ezh2* and *H3K27Me3* (input) in mouse ESCs at all genes (gray) and in genes upregulated (red) and downregulated (green) in *Dnmt3L*^{A/A} SSC. Sequence reads are plotted against the genomic distance from the gene TSS as reads per million total reads.

(B) Gene-body methylation plots of CG, CHG and CHH methylation at P_cG target genes (blue line). Methylation plots at genes with low/weak expression in E16.5 PSG (red line) as well as all RefSeq genes (black line) are shown as controls. The data indicate a lack of specific enrichment of CG or non-CG methylation at P_cG target genes in 1-dpp PSG.

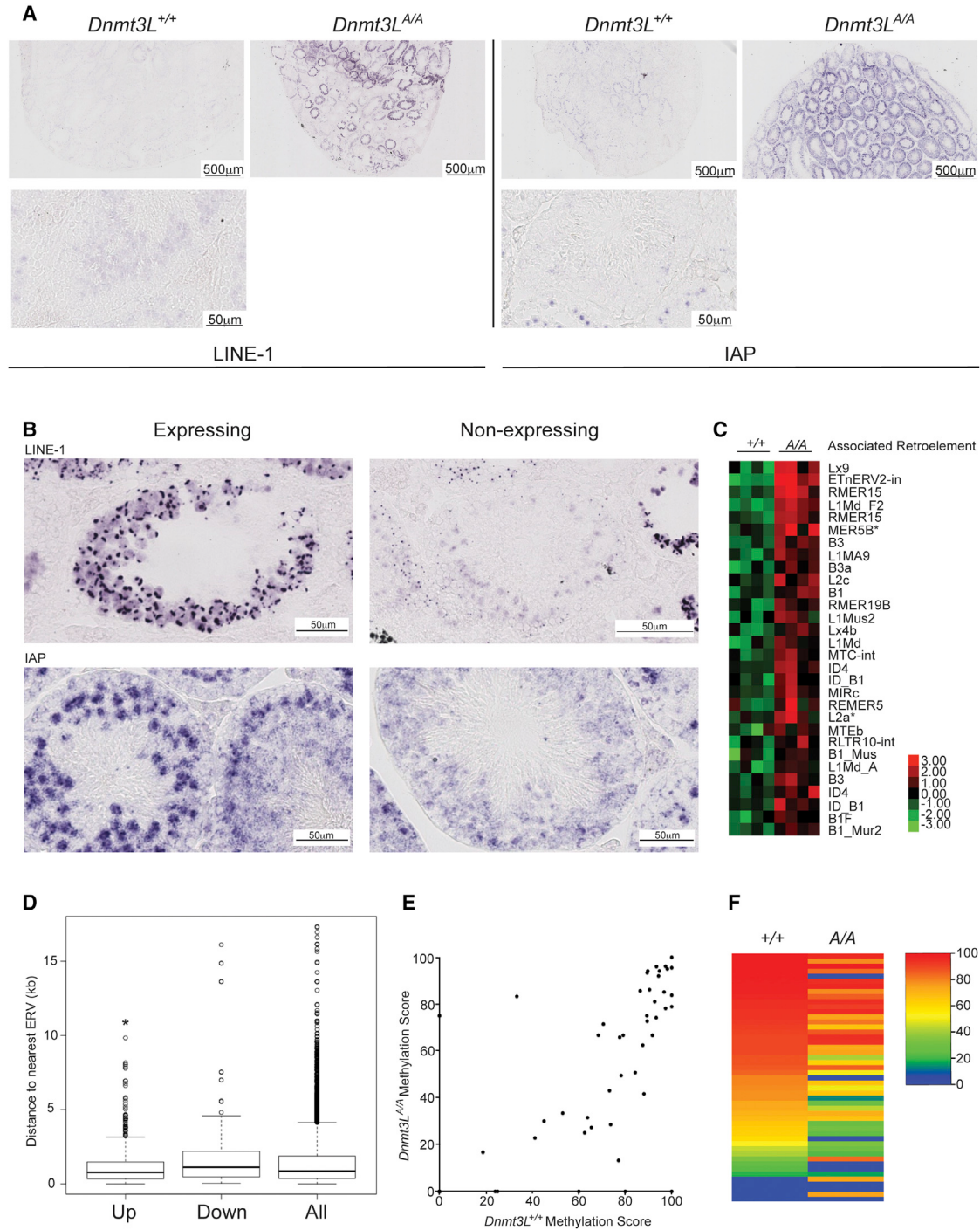


Figure 6. Analysis of Retrotransposon Expression and Methylation in *Dnmt3L*^{A/A} Testes

(A) Low- (4 \times) and high-magnification (40 \times) micrographs of testes sections from *Dnmt3L*^{+/+} and *Dnmt3L*^{A/A} animals subjected to *in situ* hybridization with the probes indicated. Tubules in *Dnmt3L*^{A/A} testes show variable retrotransposon expression (note not all tubules are positive for signal). Wild-type sections do not show a specific signal. Signal detection developed for equal duration. Images are representative of signal observed in four sections from four different animals for both genotypes.

(B) High-magnification micrographs of testes sections from *Dnmt3L*^{+/+} and *Dnmt3L*^{A/A} animals subjected to *in situ* hybridization using the probes indicated. For LINE-1 *in situ*, testes were harvested from 8-week-old and 5-week-old animals (*Dnmt3L*^{+/+} and *Dnmt3L*^{A/A}, respectively). For the IAP *in situ*, testes were harvested from 16-week-old animals; images are representative of four sections from four different animals analyzed.

(legend continued on next page)

Microarray and Data Analysis

Total RNAs were extracted using the High Pure RNA Isolation Kit (Roche Diagnostics) hybridized to Agilent SurePrint G3 Mouse GE 8x60K microarrays according to the manufacturers' protocol.

Statistical Comparisons

Unless otherwise stated, all statistical analyses were carried out using the non-parametric two-tailed Mann-Whitney test, with levels of statistical significance as indicated.

GO Analysis

Array signals were converted to \log_2 values and both genes and arrays were median centered. Rank product analysis was performed using the RankProdIt website (<http://strep-microarray.sbs.surrey.ac.uk/RankProducts/>). Significantly enriched functional gene categories were identified using DAVID (<http://david.abcc.ncifcrf.gov/>) (Huang da et al., 2009). The heatmaps shown were generated with Java TreeView (<http://jtreeview.sourceforge.net>).

ChIP-Seq

Using E14 mouse ESCs, chromatin immunoprecipitation and library construction from immunoprecipitation and input DNA followed by sequencing on an Illumina HiSeq were performed as described previously (Kanhere et al., 2012).

Methylome Data from Various Tissues

Methylome data from various tissues were downloaded from the NCBI GEO (accession number GSE42836; Hon et al., 2013).

ACCESSION NUMBERS

The data generated for this study have been deposited to the NCBI GEO and are available under accession number GSE58066.

SUPPLEMENTAL INFORMATION

Supplemental Information includes Supplemental Experimental Procedures and six figures and can be found with this article online at <http://dx.doi.org/10.1016/j.celrep.2015.01.021>.

AUTHOR CONTRIBUTIONS

S.K.T.O. conceived the project, generated the *D124* mutation, performed breeding experiments, harvested germ cell material, performed cell-sorting experiments, and conducted data analysis. V.G., A.S., and K.V. performed experiments. C.E.N. and S.T. performed bioinformatics analysis. R.G.J. performed analysis on ChIP-seq and microarray data. C.E.N. and R.J.S. performed analysis on WGBS data. D.d.R. performed testes-staging analysis. S.K.T.O. drafted and prepared the manuscript with contributions from R.J.S., R.G.J., and D.d.R.

ACKNOWLEDGMENTS

We would like to thank Attia Ashraf for assistance with genotyping and animal husbandry; Giulia Lucchiari and Fowey Harvey for their assistance with experiments; Deborah Bourc'his for her generous provision of the *Dnmt3L*-null strain, protocols, probes, and advice; Sergio A. Quezada for his patience and enthusiastic assistance with flow cytometry; Ayad Eddauodi for cell sorting; members of the Enver group for their kind assistance with flow cytometry; Austin Smith and Jenny Nichols for kindly providing the *Oct4-GiP* strain; En Li for the kind provision of *Dnmt1^{c/c}* ESCs; Masaki Okano for the kind provision of TKO ESCs; Shau-Ping Lin for provision of *Dnmt3L^{-/-}* material; Wolf Reik and Simon Andrews for kindly providing coordinates of mouse CGIs; Catherine Evans for assistance with microarrays and data analysis; UCL BLIC for assistance with data analysis; and UCL BSU for animal husbandry. We thank Mathieu Boulard, Helen Rowe, Emily Bernstein, and Rebecca Oakey for critical reading of this manuscript and useful discussions. This work was supported by a BBSRC David Phillips Fellowship (BB/H022546/1; S.K.T.O and G.V.). S.T and A.S are supported by an ERC Starting Grant (2817840-XXDNAM). R.G.J. is supported by an ERC Starting Grant (311704-ChromatinRNA). We would also like to thank the NIH (R00GM100000) for funding aspects of this study (R.J.S.).

Received: September 23, 2014
 Revised: December 12, 2014
 Accepted: January 8, 2015
 Published: February 12, 2015

REFERENCES

- Aapola, U., Liiv, I., and Peterson, P. (2002). Imprinting regulator DNMT3L is a transcriptional repressor associated with histone deacetylase activity. *Nucleic Acids Res.* 30, 3602–3608.
- Bourc'his, D., and Bestor, T.H. (2004). Meiotic catastrophe and retrotransposon reactivation in male germ cells lacking Dnmt3L. *Nature* 431, 96–99.
- Bourc'his, D., Xu, G.L., Lin, C.S., Bollman, B., and Bestor, T.H. (2001). Dnmt3L and the establishment of maternal genomic imprints. *Science* 294, 2536–2539.
- Chedin, F., Lieber, M.R., and Hsieh, C.L. (2002). The DNA methyltransferase-like protein DNMT3L stimulates de novo methylation by Dnmt3a. *Proc. Natl. Acad. Sci. USA* 99, 16916–16921.
- Clermont, Y., and Perey, B. (1957). Quantitative study of the cell population of the seminiferous tubules in immature rats. *Am. J. Anat.* 100, 241–267.
- Garcia, T., and Hofmann, M.C. (2012). Isolation of undifferentiated and early differentiating type A spermatogonia from Pou5f1-GFP reporter mice. In *Germline Development*, W.Y. Chan and L.A. Blomberg, eds. (New York: Springer), pp. 31–44.
- Goll, M.G., and Bestor, T.H. (2005). Eukaryotic cytosine methyltransferases. *Annu. Rev. Biochem.* 74, 481–514.
- Hata, K., Okano, M., Lei, H., and Li, E. (2002). Dnmt3L cooperates with the Dnmt3 family of de novo DNA methyltransferases to establish maternal imprints in mice. *Development* 129, 1983–1993.
- Hata, K., Kusumi, M., Yokomine, T., Li, E., and Sasaki, H. (2006). Meiotic and epigenetic aberrations in Dnmt3L-deficient male germ cells. *Mol. Reprod. Dev.* 73, 116–122.
- Hellman, A., and Chess, A. (2007). Gene body-specific methylation on the active X chromosome. *Science* 315, 1141–1143.

(C) Heatmap of median normalized retrotransposon-containing transcripts showing more than a 2-fold \log_2 difference in expression. Green indicates downregulation; red indicates upregulation. Only probes hybridizing to transcripts containing repeat elements are shown. Asterisk indicates probes hybridizing to transcripts that contain more than one retrotransposon. The data indicate that retrotransposons are upregulated in *Dnmt3L^{A/A}* spermatogonia at 9 dpp.

(D) Box plots showing proximity of closest proximal/upstream ERV family repeats to up- and downregulated genes in *Dnmt3L^{A/A}* SSCs. The TSSs of upregulated genes are significantly closer to proximal/upstream-located ERV/LTR family retrotransposons. Statistical analyses were carried out using the Wilcoxon rank sum test, comparing the average closest distance for each group (up- or downregulated) to that for all genes. Exact p values are 0.01279 (upregulated genes) and 0.9953 (downregulated genes).

(E) Dot plot comparing methylation levels of ERVs in proximity to upregulated genes. Note that in general, the same repeat is hypomethylated in *Dnmt3L^{A/A}* PSG compared to wild-type.

(F) Heatmap of the same data described in (E). The data indicate that ERVs in close proximity to upregulated genes in *Dnmt3L^{A/A}* SSCs are hypomethylated in PSG.

- Holz-Schietinger, C., and Reich, N.O. (2010). The inherent processivity of the human de novo methyltransferase 3A (DNMT3A) is enhanced by DNMT3L. *J. Biol. Chem.* 285, 29091–29100.
- Hon, G.C., Rajagopal, N., Shen, Y., McCleary, D.F., Yue, F., Dang, M.D., and Ren, B. (2013). Epigenetic memory at embryonic enhancers identified in DNA methylation maps from adult mouse tissues. *Nat. Genet.* 45, 1198–1206.
- Hu, J.L., Zhou, B.O., Zhang, R.R., Zhang, K.L., Zhou, J.Q., and Xu, G.L. (2009). The N-terminus of histone H3 is required for de novo DNA methylation in chromatin. *Proc. Natl. Acad. Sci. USA* 106, 22187–22192.
- Huang da, W., Sherman, B.T., and Lempicki, R.A. (2009). Systematic and integrative analysis of large gene lists using DAVID bioinformatics resources. *Nat. Protoc.* 4, 44–57.
- Illingworth, R.S., Gruenewald-Schneider, U., Webb, S., Kerr, A.R., James, K.D., Turner, D.J., Smith, C., Harrison, D.J., Andrews, R., and Bird, A.P. (2010). Orphan CpG islands identify numerous conserved promoters in the mammalian genome. *PLoS Genet.* 6, e1001134.
- Jia, D., Jurkowska, R.Z., Zhang, X., Jeltsch, A., and Cheng, X. (2007). Structure of Dnmt3a bound to Dnmt3L suggests a model for de novo DNA methylation. *Nature* 449, 248–251.
- Jurkowska, R.Z., Anspach, N., Urbanke, C., Jia, D., Reinhardt, R., Nellen, W., Cheng, X., and Jeltsch, A. (2008). Formation of nucleoprotein filaments by mammalian DNA methyltransferase Dnmt3a in complex with regulator Dnmt3L. *Nucleic Acids Res.* 36, 6656–6663.
- Kanhere, A., Hertweck, A., Bhatia, U., Gökmén, M.R., Perucha, E., Jackson, I., Lord, G.M., and Jenner, R.G. (2012). T-bet and GATA3 orchestrate Th1 and Th2 differentiation through lineage-specific targeting of distal regulatory elements. *Nat. Commun.* 3, 1268.
- Kluin, P.M., and de Rooij, D.G. (1981). A comparison between the morphology and cell kinetics of gonocytes and adult type undifferentiated spermatogonia in the mouse. *Int. J. Androl.* 4, 475–493.
- Kobayashi, H., Sakurai, T., Miura, F., Imai, M., Mochiduki, K., Yanagisawa, E., Sakashita, A., Wakai, T., Suzuki, Y., Ito, T., et al. (2013). High-resolution DNA methylome analysis of primordial germ cells identifies gender-specific reprogramming in mice. *Genome Res.* 23, 616–627.
- Ku, M., Koche, R.P., Rheinbay, E., Mendenhall, E.M., Endoh, M., Mikkelsen, T.S., Presser, A., Nusbaum, C., Xie, X., Chi, A.S., et al. (2008). Genomewide analysis of PRC1 and PRC2 occupancy identifies two classes of bivalent domains. *PLoS Genet.* 4, e1000242.
- Liao, H.F., Chen, W.S., Chen, Y.H., Kao, T.H., Tseng, Y.T., Lee, C.Y., Chiu, Y.C., Lee, P.L., Lin, Q.J., Ching, Y.H., et al. (2014). DNMT3L promotes quiescence in postnatal spermatogonial progenitor cells. *Development* 141, 2402–2413.
- Lister, R., Pelizzola, M., Dowen, R.H., Hawkins, R.D., Hon, G., Tonti-Filippini, J., Nery, J.R., Lee, L., Ye, Z., Ngo, Q.M., et al. (2009). Human DNA methylomes at base resolution show widespread epigenomic differences. *Nature* 462, 315–322.
- Lister, R., Mukamel, E.A., Nery, J.R., Urich, M., Puddifoot, C.A., Johnson, N.D., Lucero, J., Huang, Y., Dwork, A.J., Schultz, M.D., et al. (2013). Global epigenomic reconfiguration during mammalian brain development. *Science* 341, 1237905.
- Michaud, E.J., van Vugt, M.J., Bultman, S.J., Sweet, H.O., Davissón, M.T., and Woychik, R.P. (1994). Differential expression of a new dominant agouti allele (Aiap) is correlated with methylation state and is influenced by parental lineage. *Genes Dev.* 8, 1463–1472.
- Neri, F., Krepelova, A., Incarnato, D., Maldotti, M., Parlato, C., Galvagni, F., Matarese, F., Stunnenberg, H.G., and Oliviero, S. (2013). Dnmt3L antagonizes DNA methylation at bivalent promoters and favors DNA methylation at gene bodies in ESCs. *Cell* 155, 121–134.
- O'Doherty, A.M., Rutledge, C.E., Sato, S., Thakur, A., Lees-Murdock, D.J., Hata, K., and Walsh, C.P. (2011). DNA methylation plays an important role in promoter choice and protein production at the mouse Dnmt3L locus. *Dev. Biol.* 356, 411–420.
- Okano, M., Bell, D.W., Haber, D.A., and Li, E. (1999). DNA methyltransferases Dnmt3a and Dnmt3b are essential for de novo methylation and mammalian development. *Cell* 99, 247–257.
- Ooi, S.K., Qiu, C., Bernstein, E., Li, K., Jia, D., Yang, Z., Erdjument-Bromage, H., Tempst, P., Lin, S.P., Allis, C.D., et al. (2007). DNMT3L connects unmethylated lysine 4 of histone H3 to de novo methylation of DNA. *Nature* 448, 714–717.
- Ooi, S.K., Wolf, D., Hartung, O., Agarwal, S., Daley, G.Q., Goff, S.P., and Bestor, T.H. (2010). Dynamic instability of genomic methylation patterns in pluripotent stem cells. *Epigenetics Chromatin* 3, 17.
- Otani, J., Nankumo, T., Arita, K., Inamoto, S., Ariyoshi, M., and Shirakawa, M. (2009). Structural basis for recognition of H3K4 methylation status by the DNA methyltransferase 3A ATRX-DNMT3-DNMT3L domain. *EMBO Rep.* 10, 1235–1241.
- Peters, A.H., Plug, A.W., van Vugt, M.J., and de Boer, P. (1997). A drying-down technique for the spreading of mammalian meiocytes from the male and female germline. *Chromosome Res.* 5, 66–68.
- Phillips, B.T., Gassei, K., and Orwig, K.E. (2010). Spermatogonial stem cell regulation and spermatogenesis. *Philos. Trans. R. Soc. Lond. B Biol. Sci.* 365, 1663–1678.
- Sakai, Y., Suetake, I., Shinozaki, F., Yamashina, S., and Tajima, S. (2004). Co-expression of de novo DNA methyltransferases Dnmt3a2 and Dnmt3L in gonocytes of mouse embryos. *Gene Expr. Patterns* 5, 231–237.
- Schmidt, D., Schwalie, P.C., Wilson, M.D., Ballester, B., Gonçalves, A., Kutter, C., Brown, G.D., Marshall, A., Flieck, P., and Odom, D.T. (2012). Waves of retrotransposon expansion remodel genome organization and CTCF binding in multiple mammalian lineages. *Cell* 148, 335–348.
- Seisenberger, S., Andrews, S., Krueger, F., Arand, J., Walter, J., Santos, F., Popp, C., Thienpont, B., Dean, W., and Reik, W. (2012). The dynamics of genome-wide DNA methylation reprogramming in mouse primordial germ cells. *Mol. Cell* 48, 849–862.
- Shibata, H., Yoda, Y., Kato, R., Ueda, T., Kamiya, M., Hiraiwa, N., Yoshiki, A., Plass, C., Pearsall, R.S., Held, W.A., et al. (1998). A methylation imprint mark in the mouse imprinted gene Grf1/Cdc25Mm locus shares a common feature with the U2afbp-rs gene: an association with a short tandem repeat and a hypermethylated region. *Genomics* 49, 30–37.
- Shirane, K., Toh, H., Kobayashi, H., Miura, F., Chiba, H., Ito, T., Kono, T., and Sasaki, H. (2013). Mouse oocyte methylomes at base resolution reveal genome-wide accumulation of non-CpG methylation and role of DNA methyltransferases. *PLoS Genet.* 9, e1003439.
- Singh, P., Li, A.X., Tran, D.A., Oates, N., Kang, E.R., Wu, X., and Szabó, P.E. (2013). De novo DNA methylation in the male germ line occurs by default but is excluded at sites of H3K4 methylation. *Cell Rep.* 4, 205–219.
- Suetake, I., Shinozaki, F., Miyagawa, J., Takeshima, H., and Tajima, S. (2004). DNMT3L stimulates the DNA methylation activity of Dnmt3a and Dnmt3b through a direct interaction. *J. Biol. Chem.* 279, 27816–27823.
- Vergouwen, R.P., Jacobs, S.G., Huiskamp, R., Davids, J.A., and de Rooij, D.G. (1991). Proliferative activity of gonocytes, Sertoli cells and interstitial cells during testicular development in mice. *J. Reprod. Fertil.* 93, 233–243.
- Webster, K.E., O'Bryan, M.K., Fletcher, S., Crewther, P.E., Aapola, U., Craig, J., Harrison, D.K., Aung, H., Phutikanit, N., Lyle, R., et al. (2005). Meiotic and epigenetic defects in Dnmt3L-knockout mouse spermatogenesis. *Proc. Natl. Acad. Sci. USA* 102, 4068–4073.
- Xie, W., Barr, C.L., Kim, A., Yue, F., Lee, A.Y., Eubanks, J., Dempster, E.L., and Ren, B. (2012). Base-resolution analyses of sequence and parent-of-origin dependent DNA methylation in the mouse genome. *Cell* 148, 816–831.
- Ying, Q.L., Nichols, J., Evans, E.P., and Smith, A.G. (2002). Changing potency by spontaneous fusion. *Nature* 416, 545–548.
- Yoshida, S., Sukeno, M., Nakagawa, T., Ohbo, K., Nagamatsu, G., Suda, T., and Nabeshima, Y. (2006). The first round of mouse spermatogenesis is a distinctive program that lacks the self-renewing spermatogonia stage. *Development* 133, 1495–1505.
- Zhang, Y., Jurkowska, R., Soeroes, S., Rajavelu, A., Dhayalan, A., Bock, I., Rathert, P., Brandt, O., Reinhardt, R., Fischle, W., and Jeltsch, A. (2010). Chromatin methylation activity of Dnmt3a and Dnmt3a/3L is guided by interaction of the ADD domain with the histone H3 tail. *Nucleic Acids Res.* 38, 4246–4253.

Cell Reports

Supplemental Information

The Dnmt3L ADD Domain Controls Cytosine Methylation Establishment during Spermatogenesis

Georgios Vlachogiannis, Chad E. Niederhuth, Salih Tuna, Athanasia Stathopoulou, Keijo Viiri, Dirk G. de Rooij, Richard G. Jenner, Robert J. Schmitz, and Steen K.T. Ooi

Figure S1

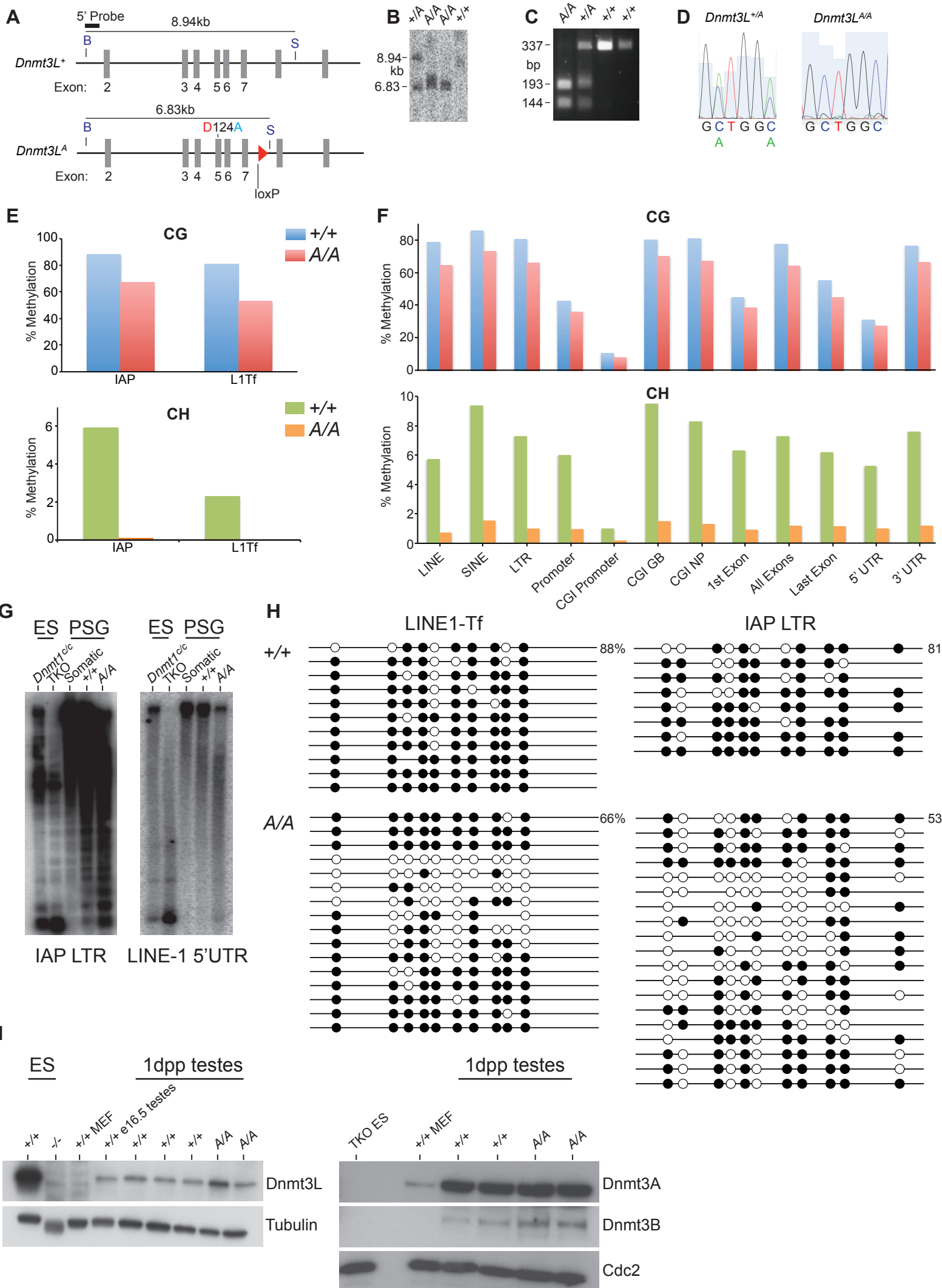


Figure S2

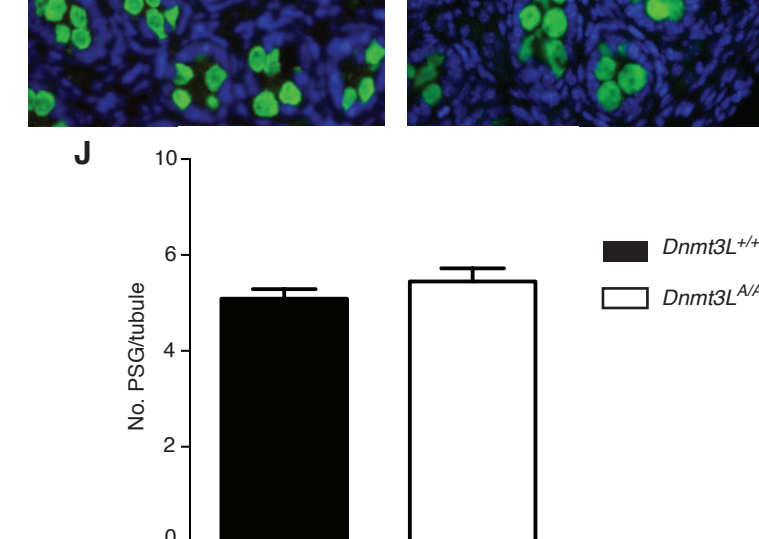
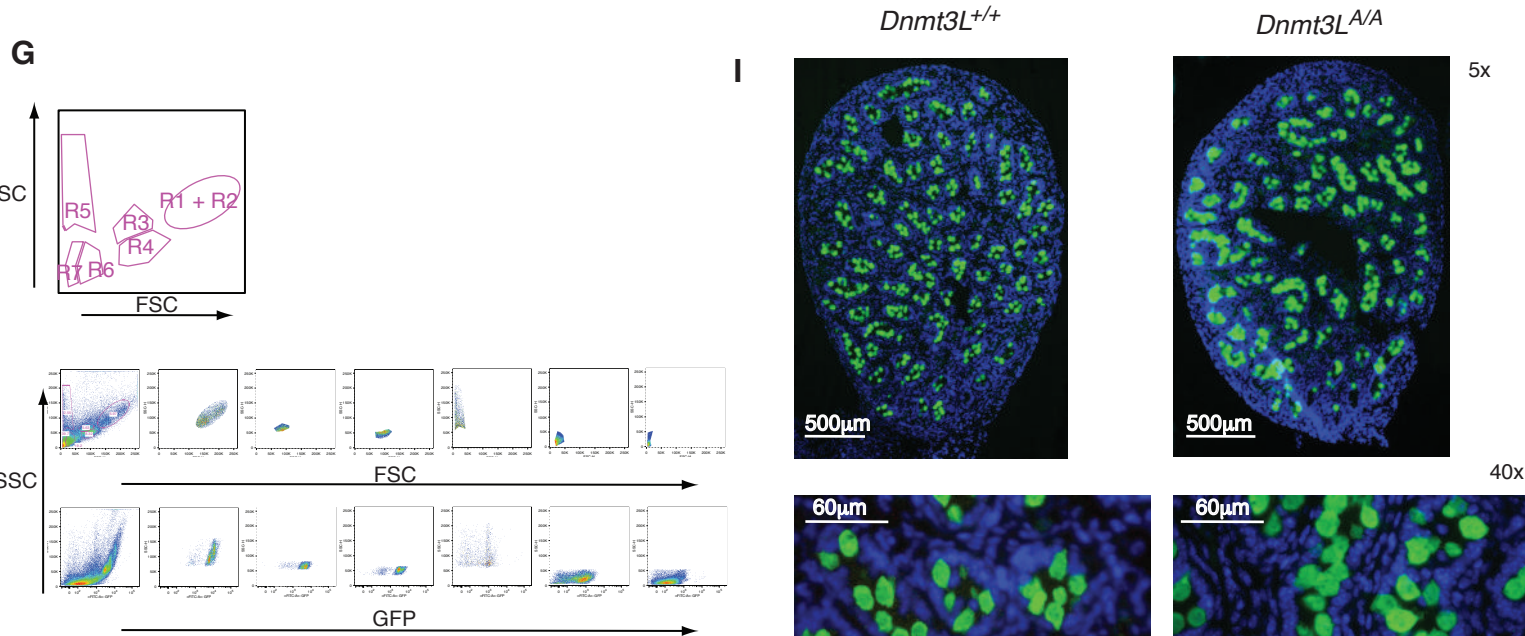
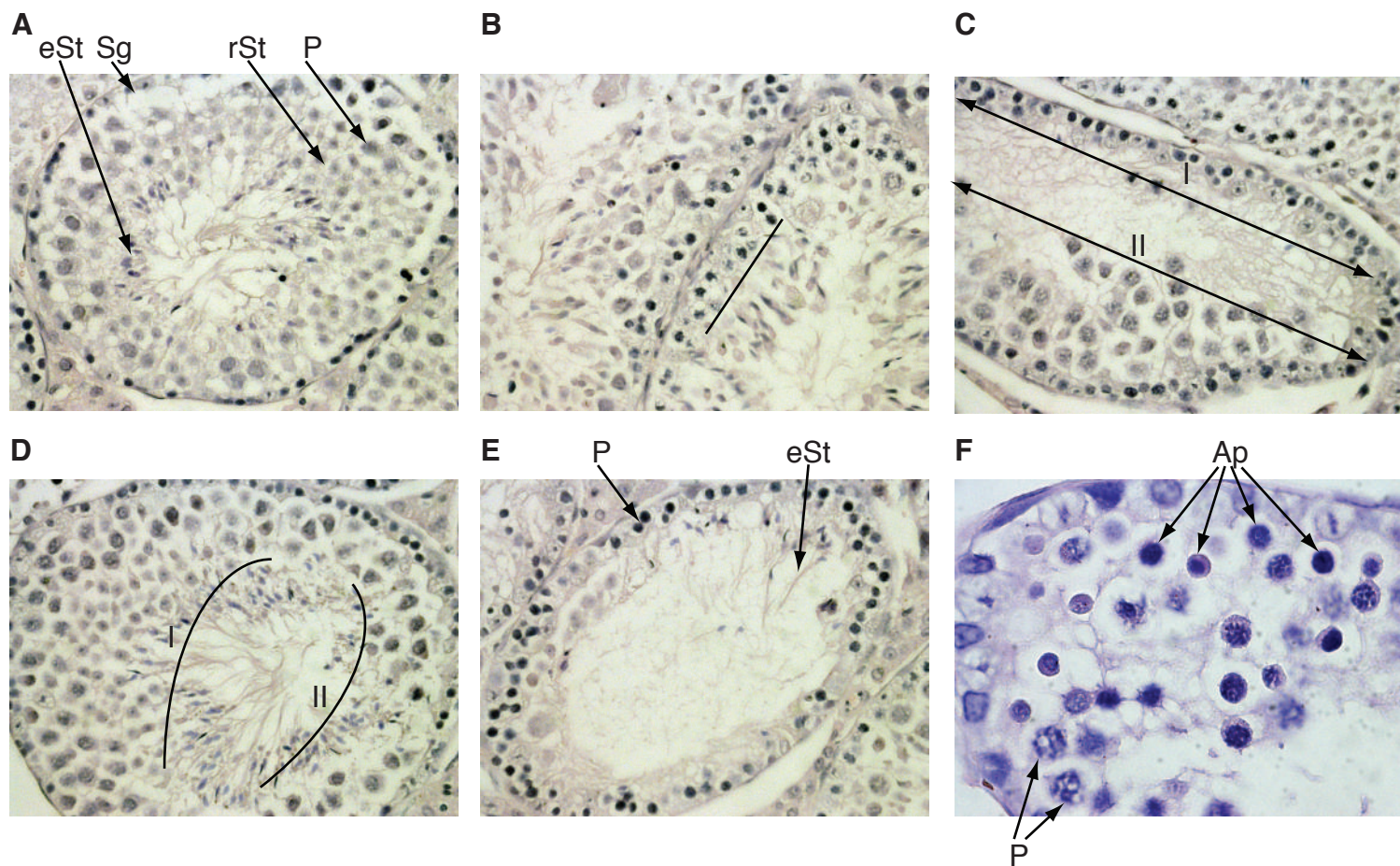


Figure S3

A Genes up-regulated in *Dnmt3L^{A/A}* spermatogonia

Positive regulation of biological process

Ref Seq ID	Gene Name
NM_008381	Inhhb
NM_013598	Kitl
NM_011766	Zfpmp2
NM_001033450	MNDA
NM_001042605	CD74
NM_008727	NPR1
NM_008225	HCLS1
NM_011905	TLR2
NM_019464	sh3glb1
NM_010658	Mafb
NM_028263	fgfbp3
NM_022018	FAM129A
NM_011691	VAV1
NM_001038845	P2RX7
NM_010288	GJA1
NM_008198	CFB
NM_007992	FBLN2
NM_008509	LOC669888
NM_008509	Lpl
NM_010186	fcgr1
NM_019971	PDGFC
NM_020008	CLEC7A
NM_007523	Bak1
NM_007609	LOC100044206
NM_007609	Bak1
NM_007609	Casp4
NM_010329	PDPN
NM_007956	Esr1
NM_013492	LOC100046120
NM_013492	clu
NM_009231	SOS1
NM_013467	aldh1a1
NM_026366	N6AMT1
NM_010400	H60a
NM_010400	H60a
NM_020044	LAT2
NM_011448	SOX9
NM_010735	Ita
NM_009380	thrB
NM_010905	NFIA
NM_007706	Gm8000
NM_007706	socs2
NM_010378	H2-Ea
NM_010378	h2-aa
NM_007536	Bcl2a1d
NM_009016	Raet1b
NM_009016	Raet1a
NM_009016	Raet1e
NM_009016	Raet1c
NM_009016	Raet1d
NM_011445	Sox6
NM_008329	Ifi204
NM_011340	Serpinf1

B Genes down-regulated in *Dnmt3L^{A/A}* spermatogonia

Cellular developmental process

Ref Seq ID	Gene Name
NM_008091	GATA3
NM_178280	sall3
NM_008267	HOXB13
NM_016889	Insm1
NM_008982	PTPRJ
NM_008982	Gm13767
NM_008982	Gm13768
NM_148935	FOXN4
NM_177259	dab1
NM_010053	dlx1
NM_008700	NKX2-5
NM_008499	Lhx5
NM_021459	Isl1
NM_010800	bhlha15
NM_008471	KRT19
NM_145492	Zfp521
NM_008899	pou3f2
NM_177638	Crb3
NM_008259	foxa1
NM_008259	LOC100047556
NM_011097	pitX1
NM_008257	HMX3
NM_007628	CCNA1
NM_010203	FGF5
NM_010449	hoxa1
NM_033327	Zfp423
NM_033327	LOC100046333
NM_023478	Upk3a
NM_054053	GPR98
NM_010054	Dlx2
NM_010278	GFI1
NM_001142732	TTLL3
NM_027572	SLC22A16
NM_001171512	obscn
NM_007865	DLL1
NM_010713	LHX8

Cell fate commitment

Ref Seq ID	Gene Name
NM_008259	foxa1
NM_008259	LOC100047556
NM_008091	GATA3
NM_010054	Dlx2
NM_021459	Isl1
NM_011097	pitX1
NM_010278	GFI1
NM_148935	FOXN4
NM_010053	dlx1
NM_007865	DLL1
NM_010713	DLL1

Positive regulation of cellular process

Ref Seq ID	Gene Name
NM_008381	Inhhb
NM_013598	Kitl
NM_011766	Zfpmp2
NM_001033450	MNDA
NM_001042605	CD74
NM_008727	NPR1
NM_008225	HCLS1
NM_011905	TLR2
NM_019464	sh3glb1
NM_010658	Mafb
NM_028263	fgfbp3
NM_022018	FAM129A
NM_011691	VAV1
NM_001038845	P2RX7
NM_010288	GJA1
NM_008198	CFB
NM_007992	FBLN2
NM_008509	LOC669888
NM_008509	Lpl
NM_010186	fcgr1
NM_019971	PDGFC
NM_020008	CLEC7A
NM_007523	Bak1
NM_007609	LOC100044206
NM_007609	Casp4
NM_013492	LOC100046120
NM_013492	clu
NM_009231	SOS1
NM_013467	aldh1a1
NM_001042605	CD74
NM_019464	sh3glb1
NM_011448	SOX9
NM_010735	Ita
NM_001038845	P2RX7
NM_007536	Bcl2a1d
NM_008846	Gm7298
NM_008846	cpamd8
NM_029733	2010005H15Rik
NM_011340	Serpinf1

Endopeptidase inhibitor activity

Ref Seq ID	Gene Name
NM_001082547	Gm5483
NM_009977	Cst7
NM_01082546	Stfa3
NM_001082546	BC100530
NM_198028	SERPINPB10
NM_001012725	Wfdc6b
NM_001167705	Serpina3a
NM_007536	Bcl2a1d
NM_172953	Serpina5
NM_008645	mug1
NM_008645	Gm7298
NM_008646	cpamd8
NM_029733	2010005H15Rik
NM_011340	Serpinf1

Regulation of apoptosis

Ref Seq ID	Gene Name
NM_007523	Bak1
NM_013598	Kitl
NM_007956	Esr1
NM_007609	LOC100044206
NM_013492	LOC100046120
NM_013492	clu
NM_013467	aldh1a1
NM_001042605	CD74
NM_019464	sh3glb1
NM_011448	SOX9
NM_010735	Ita
NM_001038845	P2RX7
NM_007536	Bcl2a1d
NM_008329	Ifi204
NM_010186	fcgr1

Multicellular organismal development

Ref Seq ID	Gene Name
NM_008091	GATA3
NM_001159407	b3gnt5
NM_178280	sall3
NM_016889	Insm1
NM_008982	PTPRJ
NM_008982	Gm13767
NM_008982	Gm13768
NM_148935	FOXN4
NM_177259	dab1
NM_010053	dlx1
NM_008700	NKX2-5
NM_008499	Lhx5
NM_021459	Isl1
NM_024230	SMTNL1
NM_008471	KRT19
NM_145492	Zfp521
NM_009877	CDKN2A
NM_010096	EBF3
NM_008899	pou3f2
NM_177638	Crb3
NM_011536	TBX4
NM_008259	foxa1
NM_008259	LOC100047556
NM_011097	pitX1
NM_008257	HMX3
NM_015768	Prok2
NM_019448	Dnmt3l
NM_019448	LOC100048887
NM_139218	dppA3
NM_139218	Gm6269
NM_010449	hoxa1
NM_007628	CCNA1
NM_033327	Zfp423
NM_033327	LOC100046333
NM_010053	dlx1
NM_008700	NKX2-5
NM_010054	Dlx2
NM_021459	Isl1
NM_008499	Lhx5
NM_013914	SNAI3
NM_009877	CDKN2A
NM_133659	ERG
NM_008899	pou3f2
NM_011536	TBX4
NM_010713	LHX8

Transcription regulator activity

Ref Seq ID	Gene Name
NM_010054	Dlx2
NM_008499	Lhx5
NM_021459	Isl1
NM_008259	LOC100047556
NM_008259	LOC100047556
NM_008091	GATA3
NM_008257	HMX3
NM_011097	pitX1
NM_008267	HOXB13
NM_148935	FOXN4
NM_010449	hoxa1
NM_033327	Zfp423
NM_033327	LOC100046333
NM_010053	dlx1
NM_008700	NKX2-5
NM_010054	Dlx2
NM_021459	Isl1
NM_008499	Lhx5
NM_013914	SNAI3
NM_009877	CDKN2A
NM_133659	ERG
NM_008899	pou3f2
NM_011536	TBX4
NM_010713	LHX8

Homeobox, conserved site

Ref Seq ID	Gene Name
NM_008259	foxa1
NM_008259	LOC100047556
NM_008091	GATA3
NM_008257	HMX3
NM_011097	pitX1
NM_008257	HMX3
NM_015768	Prok2
NM_019448	Dnmt3l
NM_019448	LOC100048887
NM_139218	dppA3
NM_139218	Gm6269
NM_010449	hoxa1
NM_007628	CCNA1
NM_033327	Zfp423
NM_033327	LOC100046333
NM_01033415	Shisa3
NM_023478	Upk3a
NM_054053	GPR98
NM_010054	Dlx2
NM_01146268	Pdgfrb
NM_010278	GFI1
NM_027572	SLC22A16
NM_001171512	obscn
NM_007865	DLL1
NM_010713	LHX8

Figure S4

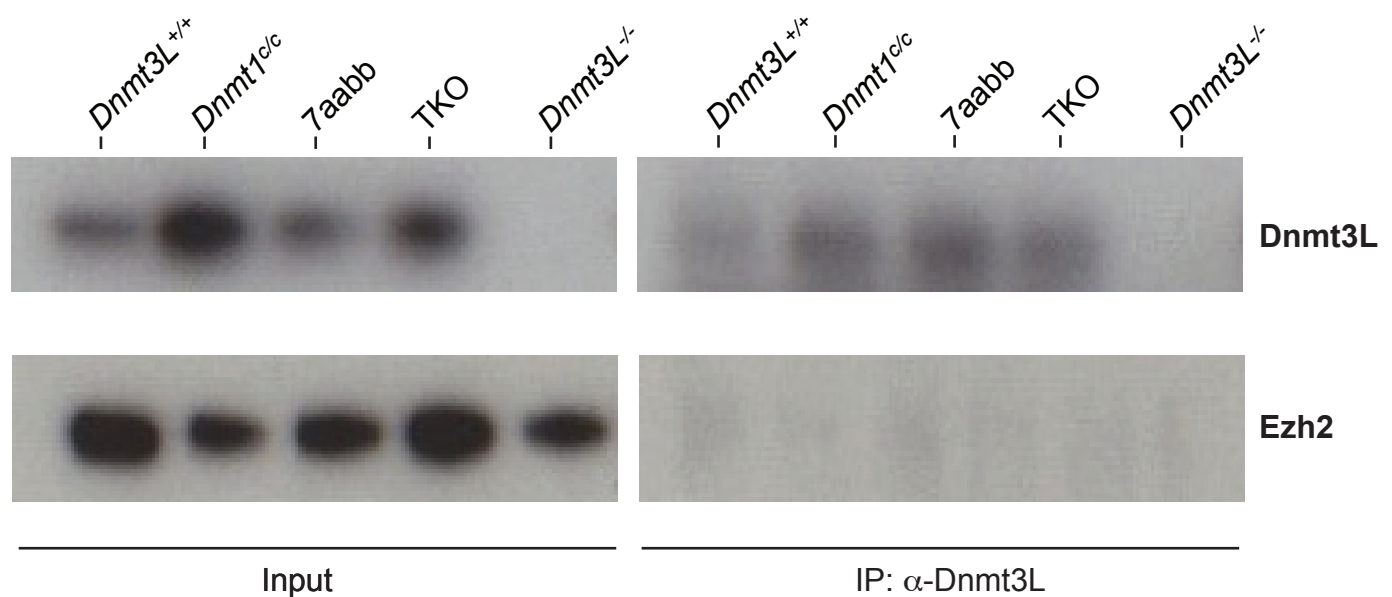
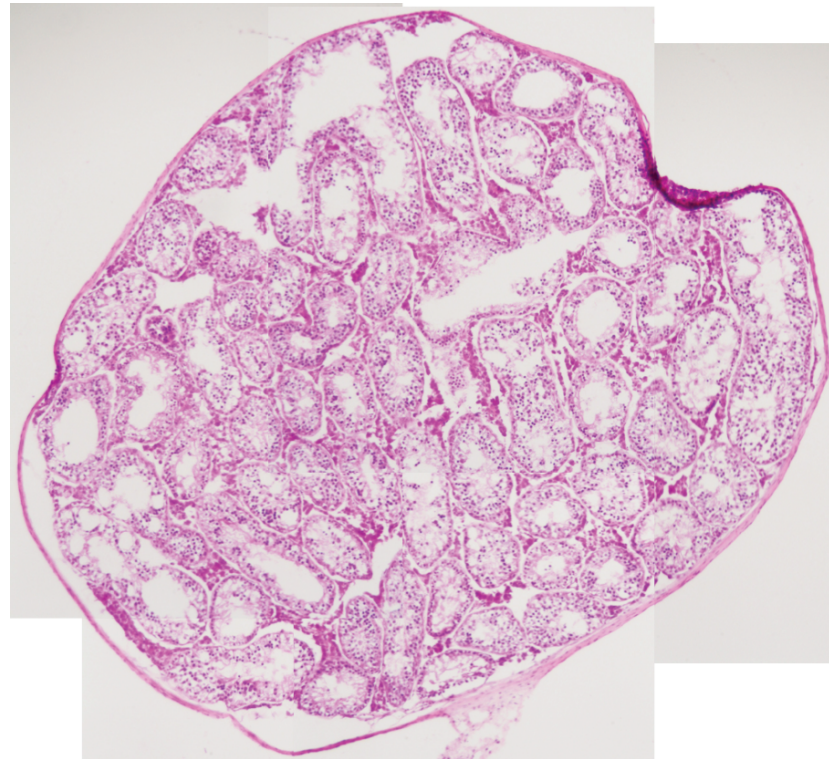
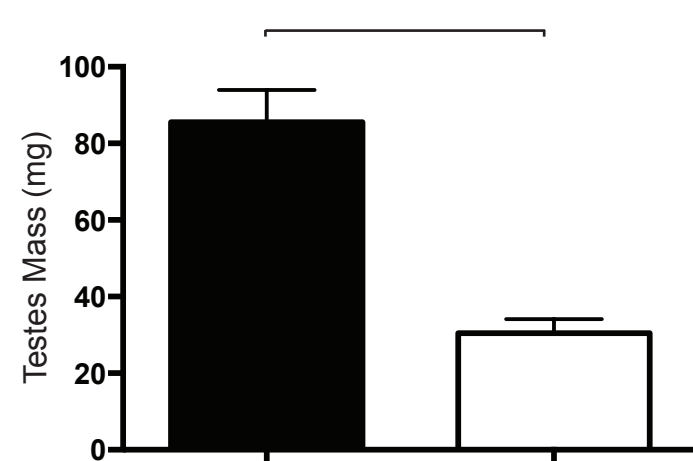


Figure S5

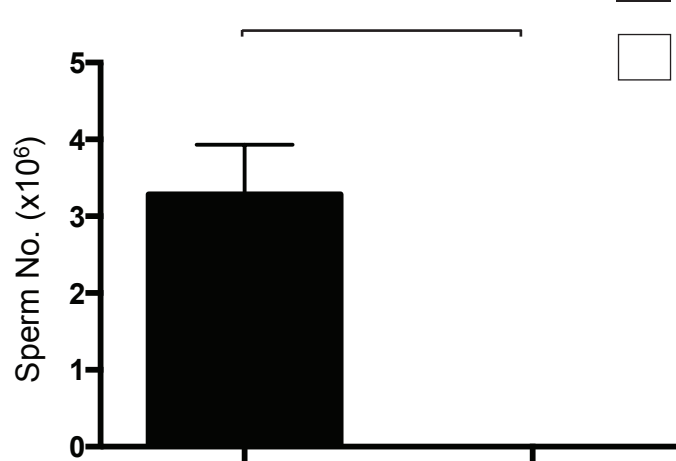
A



B

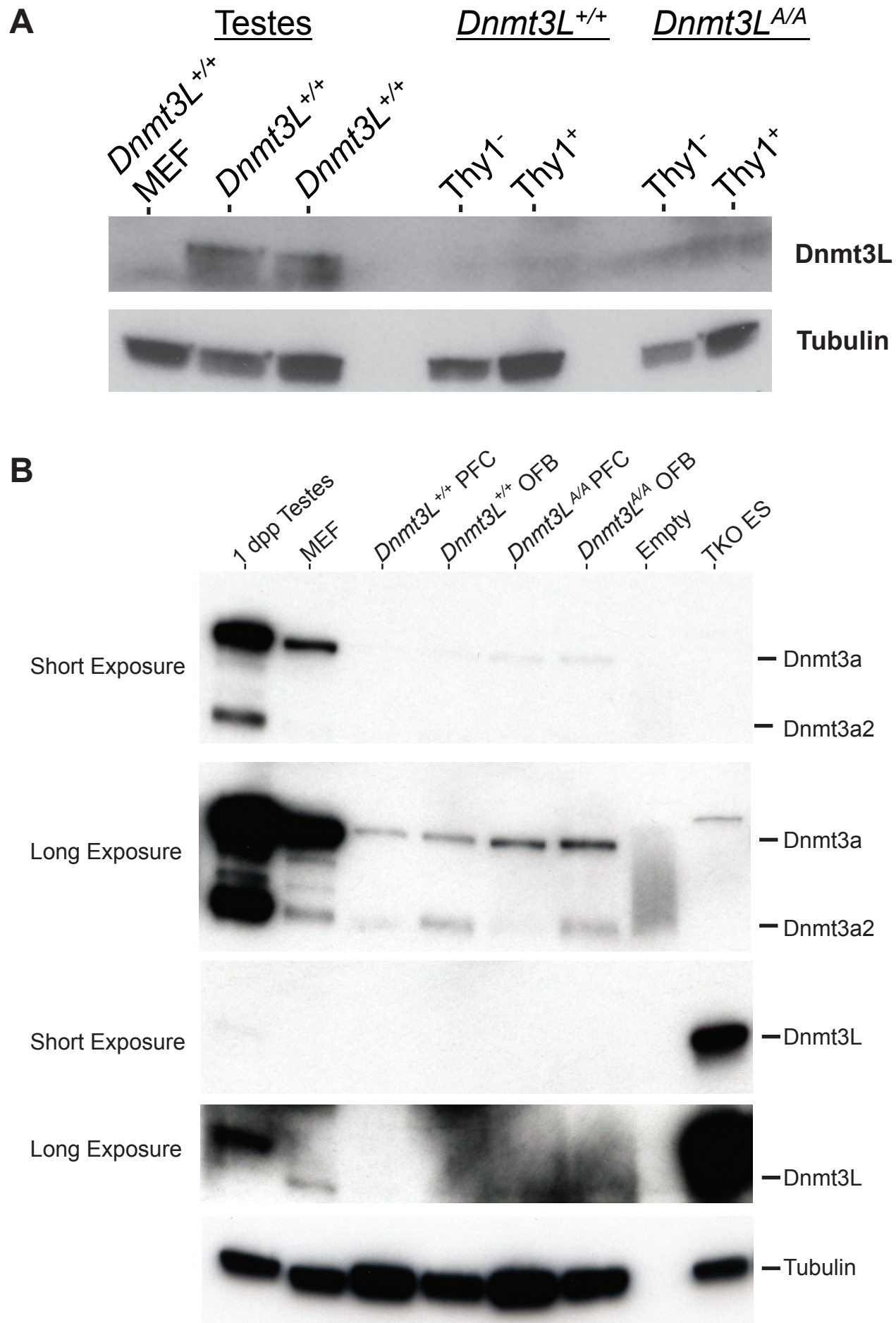


C



$Dnmt3L^{+/+}$
 $Dnmt3L^{-/-}$

Figure S6



Supplemental Figure Legends

Figure S1 (related to Figure 1): Generation of *Dnmt3L*^{A/A} animals and methylation analysis. **A** Targeting strategy used to introduce and detect the *D124A* mutation at the endogenous *Dnmt3L* locus. Identification of targeted clones involved digestion with BamHI (B) and Spel (S) restriction enzymes. **B** Diagnostic Southern blot using the probe indicated in **A** showing the detection of the targeted allele. **C** Agarose gel electrophoresis of PCR products used to distinguish between wild type (*Dnmt3L*^{+/+}) and mutant (*Dnmt3L*^{A/A}) alleles. As well as introducing the A to C transversion resulting in the *D124A* mutation, the targeting construct also introduced a silent A to C transversion resulting in the generation of an *MscI* restriction site. PCR across this site followed by restriction digestion of by *MscI* generates either an undigested fragment from the *Dnmt3L*⁺ allele (337bp,) or two digested fragments from the *Dnmt3L*^A allele (193bp and 144bp). **D** Sequencing traces of PCR amplicons across the *D124A* mutation site using genomic DNA extracted from tail biopsies. Note the presence of 2 peaks in the left panel indicative of heterozygosity for the *D124A* mutation. The right panel indicates the animal is homozygous for the *D124A* mutation. **E** Bar graphs indicating percentage methylation at CG and CH contexts in bisulphite-converted amplicons. Results indicate reduced CG and non-CG methylation at IAP and L1Tf retrotransposons. **F** Percentage CG and CH methylation in different compartments indicated. Data indicate that the *D124A* mutation causes reduced methylation in all compartments analysed. **G** Methylation-sensitive Southern Blot data on DNA purified from 1dpp testes. As controls for un- and hypomethylated DNA, DNA extracted from *Dnmt1*^{c/c} and *Dnmt1*^{-/-}*Dnmt3a*^{-/-}*Dnmt3b*^{-/-} (TKO) ES cells was also

included. *Dnmt1*^{c/c} ES cells are deficient for the maintenance methyltransferase Dnmt1; TKO cells are deficient for all known methyltransferases. Tail-biopsy DNA (somatic) from wild-type animals was used as a normally methylated control. Note both the presence and intensity of the lower molecular weight signal in the lanes containing DNA from 1dpp *Dnmt3L*^{A/A} testes DNA. **H** Bisulphite sequencing data from FACS-purified prospermatogonia from 1dpp testes, different regions are as indicated. Note the presence of unmethylated, partially methylated and fully methylated sequences in DNA from *Dnmt3L*^{A/A} animals. IAP methylation percentages are 81% (*Dnmt3L*^{+/+}) and 53% (*Dnmt3L*^{A/A}). LINE1-Tf methylation percentages are 88% (*Dnmt3L*^{+/+}) and 66% (*Dnmt3L*^{A/A}). **I** Western blot data examining expression of Dnmt3a, Dnmt3b and Dnmt3L in RIPA extracts from 1dpp testes and other cells as indicated. e16.5 material indicates testes. Levels of tubulin and Cdc2 expression were used as loading controls. The data indicates that the D124A mutation does not affect expression of Dnmt3 family members.

Figure S2 (related to Figure 3): Characterisation of *Dnmt3L*^{A/A} tubules displaying normal and abnormal development. A Example of a normal tubule with the various spermatogenic stages present. **B** Stage XI tubules, however the tubule on the right lacks diplotene spermatocytes (area marked by line). **C** Tubule with cells blocked at two stages; region I indicates germ cells that developed no further than the zygotene stage (stage IV). On the opposite side of the same tubule in region II, development is blocked at the round spermatid stage. **D** Partially normal tubule that has all developmental

stages (region I). However in region II, despite the presence of elongating spermatids, round spermatids are absent. **E** Tubule containing mainly young pachytene spermatocytes. Despite the presence of elongating spermatids, no round spermatids are present. **F** Stage IV tubule where majority of spermatocytes are undergoing apoptosis, although pachytene spermatocytes are also present. **G** Top panel indicates gates used to distinguish different spermatogenic stages by flow cytometry based on forward scatter height (FSC-H) and side scatter height (SSC-H) as described by Malkov et al. (Malkov et al., 1998). These were then used to position gates based on GFP expression. Briefly, testicular cells are subdivided into 7 populations; R1 and R2 represent cells at G2 of mitosis as well as primary spermatocytes undergoing prophase I. R3 and R4 represent diploid cells, which includes somatic (Sertoli, Leydig and peritubular cells) as well as germ cells (spermatogonia at mitotic G1, pre-leptotene spermatocytes prior to premeiotic S phase and secondary spermatocytes between meiosis I and II). R5 represents elongated and condensed spermatozoa, and R6 and R7 represent early round, elongating and condensing spermatids. **H** Representative FACS-density plots of testicular germ cells. Panel I shows a representative distribution of spermatogenic cells in wild-type animals. Panel II and III are both plots of cells from *Dnmt3L*^{AA} animals demonstrating either a normal wild type like distribution (Panel II) or severe reductions (Panel III). **I** Low (5x) and high (40x) magnification micrographs of 1dpp testes from *Oct4-GiP*⁺ and *Dnmt3L*^{AA} *Oct4-GiP*⁺ animals stained with anti-GFP antibody. Nuclei were counterstained with DAPI. Bar graphs represent average number of GFP⁺ prospermatogonia per seminiferous tubule (*Dnmt3L*^{+/+} = 5.09, *Dnmt3L*^{AA} =

5.45). 100 tubules counted per genotype. No significant difference was observed (exact p value: 0.8240). The data indicates that the number of seeding spermatogonia in seminiferous tubules is unaffected in *Dnmt3L*^{A/A} animals.

Figure S3 (related to Figure 4): List of genes deregulated in different GO classes in *Dnmt3L*^{A/A} spermatogonia. A List of genes upregulated. **B** List of genes downregulated.

Figure S4 (related to Discussion): Absence of detectable Ezh2 in complex with Dnmt3L in ES cells. Western blot of whole cell lysates before and after immunoprecipitation with anti-Dnmt3L antibody, probed with either anti-Dnmt3L or Ezh2 antibodies. 7aabb indicates *Dnmt3A*^{-/-}*Dnmt3B*^{-/-} ES cells.

Figure S5 (related to Discussion): Complete penetrance of sterility phenotype caused by hemizygosity of *D124A* mutation. A 10x micrograph image of H&E stained section of paraformaldehyde-fixed and OCT-embedded testes from a *Dnmt3L*^{A/-} male animal (Age, 11 weeks). Image shown is representative of eight testes sections analyses from eight mutant animals. Note that all seminiferous tubules are defective, analogous to *Dnmt3L*-null testes. **B** Bar graph showing testes mass and sperm counts from *Dnmt3L*^{A/+} and *Dnmt3L*^{A/-} (n = 8, Age: 8-12 weeks) animals. Graphs show mean +/- S.D. Exact p values: p<0.0001 (testes mass); p = 0.001 (sperm count). Note that all *Dnmt3L*^{A/-} animals were azoospermic.

Figure S6 (related to Discussion): Lack of detectable Dnmt3L protein expression in SSC and juvenile prefrontal cortex. **A** Western blot data showing absence of detectable Dnmt3L protein expression in RIPA extracts from FACS-purified Thy1⁺ and Thy1⁻ SSCs purified from 9dpp *Dnmt3L*^{AA} animals. Note abundant expression of Dnmt3L protein in 1dpp whole testes. Expression of tubulin was used as a loading control. **B** Western blot data showing absence of detectable Dnmt3L protein expression in RIPA extracts from prefrontal cortex (PFC) and olfactory bulb (OB) extracted from wild type (46dpp) and *Dnmt3L*^{AA} (33dpp) animals. Note abundant expression of Dnmt3L protein in 1dpp whole testes and ES cells. Expression of tubulin was used as a loading control.

Supplemental Experimental Procedures

Methylation-sensitive Southern blot

Kit purified genomic DNA was digested using HpaII restriction endonuclease for six hours before separation by gel electrophoresis. Following resolution, DNA was depurinated, denatured and neutralized before overnight transfer onto Nytran membrane. The next day, DNA was cross-linked by UV light before incubating in Prehybridisation Solution for a minimum of two hours at 65°C. Radio labeled probes were added to membranes and incubated over night at 65°C. The next day, membranes were washed to remove unbound probe before detection of radioactive signal using a PhosphorImager screen.

Bisulphite sequencing

Kit-purified DNA from FACS-purified prospermatogonia extracted from 1dpp testes was bisulphite converted using the EZ DNA Methylation Lightning Kit (Zymo Research) according to the manufacturers protocol. Post conversion, DNA was used for PCR. Amplicons were resolved by gel electrophoresis and DNA was purified using the GeneJET Gel Extraction Kit (Thermofisher) prior to cloning using the CloneJET PCR Cloning Kit (Thermofisher) according to the manufacturers protocol before transformation of cloned products into heat-shock competent bacteria. The next day, colony PCRs were performed (25 μ l volume) and clones containing amplicons of the expected sizes were identified by gel electrophoresis. Exo-SAP was added to the remaining

volume of positive clones before subjecting to Sanger sequencing. Analysis of bisulphite data was performed using QUMA software (<http://quma.cdb.riken.jp>).

Antibodies

For western blot, the following antibodies were used: anti-Dnmt3a rabbit polyclonal (SC-20703, Santa Cruz Biotechnologies), anti-Dnmt3b mouse monoclonal (SC-52922, Santa Cruz Biotechnologies), anti-Cdc2 (PSTAIRE) rabbit polyclonal (SC053, Santa Cruz Biotechnologies), anti-Dnmt3L rabbit polyclonal (12309, Cell Signaling Technology), anti-Tubulin mouse monoclonal (T6199, Sigma-Aldrich), anti-Ezh2 mouse monoclonal (3147, Cell Signaling Technology). For purification of Thy1⁺ SSCs, APC-conjugated anti-CD90.2 (Thy1.2) (53-2.1, Biolegend) was used.

ChIP-Seq Metagene Analysis

ChIP-Seq for Suz12 and H3K27me3 was performed in E14 ES cells with the antibodies ab12073 and ab6002 (Abcam), respectively, using methods reported previously (Kanhere et al., 2012). ChIP-Seq data for Ezh2 was downloaded from GEO (GSM327668, (Ku et al., 2008). Sequence reads were aligned using Bowtie (default settings). Wig files were generated by calculating tag density in 10bp windows and normalized to reads per million total reads using in-house R scripts. The data for ChIP sequencing runs were then background corrected (input for Suz12 ChIP, H3 for H3K27me3 ChIP)

and average-binding profiles across TSSs (for all genes, up-regulated genes and down-regulated genes in *Dnmt3L*^{A/A} SSCs) plotted using a custom R script. PRC2 target genes were selected as those bound by both Suz12 and Ezh2 in mESC according to the data of Ku et al., (Ku et al., 2008). Those associated with H3K27me3 in mESC as defined by both Mikkelsen et al. (Mikkelsen et al., 2008) and Lienert et al. (Lienert et al., 2011).

Analysis of repeat proximity to differentially expression genes

The TSS locations of all genes and repeats were extracted and downloaded from the mm9 build of the mouse reference genome from the UCSC genome browser (<http://genome.ucsc.edu>). Repeats were filtered into 3 groups (LINE, LTR and SINE), using the repeat classifications provided by RepeatMasker (<http://www.repeatmasker.org>). For each TSS, the distance to the closest repeat was calculated using bedtools (closestBed option, bedtools v2.18.1) (<http://bedtools.readthedocs.org/en/latest/>). This algorithm calculates the distance from TSS to the ends of the repeats and reports on the closest distance. Using R, box plots were plotted of distances to closest repeats for genes that were either up- or down-regulated in *Dnmt3L*^{A/A} SSCs. Closest distances for all genes were also plotted as a control. Significance was calculated using the Wilcoxon Rank Sum test, comparing average repeat distances for up or down-regulated genes to average repeat distance for all genes.

MethylC-seq library preparation and sequencing

200ng of genomic DNA (gDNA) along with 5ng of spiked in lambda DNA was sonicated in 130 μ l nuclease free water to 200bp fragments using a Covaris S-2 sonicator (Covaris Inc.). Large fragment removal was accomplished by mixing magnetic purification beads (MPB - see below) with sonicated gDNA at a volume ratio of 0.6X and incubation for 10 minutes at room temperature. After 10 minutes samples were moved to a magnetic plate to separate beads from solution. Supernatant was removed from beads and added to a volume of MPB at a 0.8 ratio compared to original gDNA solution volume to create a total MPB to gDNA volume ratio of 1.4; tubes containing beads and large fragment DNA were discarded. Samples were then cleaned per described purification methods (See below).

Fragmented gDNA from sonication was repaired using End-It DNA End-Repair Kit (Epicentre) according to manufacturer's instructions. A-tails were added to blunt ended fragments during a 30 minute 37°C incubation using Klenow 3'-5' exonuclease and dA-Tailing Buffer (New England Biolabs). Methylated NEXTflex DNA adapters (Bioo Scientific) were ligated via 16 hour, 16°C incubation with T4 DNA ligase and ligation buffer (New England Biolabs). Post ligation, samples underwent two clean up procedures and then were subject to bisulfite conversion using a MethylCode kit, as per manufacturer's instructions. Libraries were amplified with eight cycles of PCR using Kapa HiFi Uracil+ Hotstart DNA Polymerase (Kapa Biosystems).

MPB were mixed with samples at a volume ratio of 1.4:1 prior to adapter

ligation and 1.0:1.0 post adapter ligation. To wash, MPB solution was mixed with samples by pipetting and left at room temperature for 10 minutes. After, samples were moved to magnets to isolate magnetic beads from solution. Supernatant was removed and beads were washed twice with 80% ethanol. Samples were removed from magnets and DNA was eluted of beads into 10mM Tris-HCl pH 8.0. and left at room temperature for 10 minutes. Sequencing was performed on an Illumina NextSeq 500.

Alignment and analysis of MethylC-seq data

Raw FASTQ files were trimmed for adapter a sequence, preprocessed to remove low quality reads and aligned to the mm10 reference genome as previously described in (Lister et al., 2011). Inefficiencies in the sodium bisulfite conversion reaction are calculated by measuring the fraction of methylated base calls detected in the spiked-in Lambda control DNA (which is unmethylated). This non-conversion rate is used as the null hypothesis using a binomial test to determine if a cytosine is methylated and the resulting p-values are corrected for multiple testing using Benjamini-Hochberg with an FDR cut off of 5%. For *Dnmt3L^{+/+}* and *Dnmt3L^{A/A}*, a total of 408,932,744 (~15x genome coverage) and 299,546,426 (~11x genome coverage) reads were uniquely and non-clonally aligned to the reference genome, respectively. The sodium bisulphite conversion rates for the *Dnmt3L^{+/+}* and *Dnmt3L^{A/A}* MethylC-seq libraries were 99.56 % and 99.52%, respectively. Data for somatic mouse tissues were obtained from the following study (Hon et al., 2013).

Calculation of methylation levels

All methylation levels that were calculated from WGBS data were determined using the weighted methylation levels described in (Schultz et al., 2012)

Differential gene expression analysis in prospermatogonia

RNA-seq data from e16.5 prospermatogonia was previously described by Seisenberger et al. (Seisenberger et al., 2012) and obtained from the European Nucleotide Archive (ERP001953). To identify PSG specific transcripts, RNA-seq data from mouse lung fibroblasts (GEO Accession number GSM521651) was used for comparison. A list of highly and lowly expressed genes was obtained using the Genestack Platform (<http://platform.genestack.org>). A binomial test was used to determine if genes were differentially expressed between e16.5 prospermatogonia and mouse embryonic lung fibroblast and the resulting p-values were corrected for multiple testing using the Benjamini and Hochberg correction with an FDR cut off of 5%. All raw data, processed files and final outputs are available on Genestack Platform and can be shared upon request for viewing or reproducing the analyses reported.

Flow cytometric analysis of GFP⁺ germ cells

Single cell suspensions of mouse testicular cells enriched for seminiferous epithelium cells (principally germ and Sertoli cells) were isolated from age-

matched wild-type and *Dnmt3L*^{A/A} animals carrying the *Oct4-GiP* reporter using the method described by Garcia and Hofmann (Garcia and Hoffman, 2012). Live cells were identified using the Annexin V: PE Apoptosis detection kit (BD Biosciences), according to the manufacturers protocol. Cells were analysed on a BD Fortessa Flow Cytometer (BD Biosciences) and analysis performed using FlowJo Cytometric Analytical software (FlowJo).

GFP staining of 1dpp testes sections

1dpp/newborn animals were sacrificed and testes were harvested from male animals and fixed and frozen in OCT as previously described. Sections mounted on slides were fixed for 10 minutes at room temperature with 4% PFA, followed by two washes in PBS + 0.1% Triton X-100 (PBT). Slides were then blocked in Blocking Solution (PBT + 1% BSA +0.15% Glycine) for one hour at room temperature before addition of anti-GFP antibody in Blocking Solution and incubating overnight at 4°C. The next day, slides were washed with PBT several times before incubation with secondary antibody (details) and incubated in the dark at room temperature for one hour. Slides were then washed several times with PBT before mounting. Analysis and image capture was performed on a Zeiss Axio Observer Z1 fluorescent microscope.

Supplemental References

- Hon, G.C., Rajagopal, N., Shen, Y., McCleary, D.F., Yue, F., Dang, M.D., and Ren, B. (2013). Epigenetic memory at embryonic enhancers identified in DNA methylation maps from adult mouse tissues. *Nature genetics* 45, 1198-1206.
- Kanhere, A., Hertweck, A., Bhatia, U., Gokmen, M.R., Perucha, E., Jackson, I., Lord, G.M., and Jenner, R.G. (2012). T-bet and GATA3 orchestrate Th1 and Th2 differentiation through lineage-specific targeting of distal regulatory elements. *Nature communications* 3, 1268.
- Ku, M., Koche, R.P., Rheinbay, E., Mendenhall, E.M., Endoh, M., Mikkelsen, T.S., Presser, A., Nusbaum, C., Xie, X., Chi, A.S., et al. (2008). Genomewide analysis of PRC1 and PRC2 occupancy identifies two classes of bivalent domains. *PLoS genetics* 4, e1000242.
- Lienert, F., Mohn, F., Tiwari, V.K., Baubec, T., Roloff, T.C., Gaidatzis, D., Stadler, M.B., and Schubeler, D. (2011). Genomic prevalence of heterochromatic H3K9me2 and transcription do not discriminate pluripotent from terminally differentiated cells. *PLoS genetics* 7, e1002090.
- Lister, R., Pelizzola, M., Kida, Y.S., Hawkins, R.D., Nery, J.R., Hon, G., Antosiewicz-Bourget, J., O'Malley, R., Castanon, R., Klugman, S., et al. (2011). Hotspots of aberrant epigenomic reprogramming in human induced pluripotent stem cells. *Nature* 471, 68-73.
- Malkov, M., Fisher, Y., and Don, J. (1998). Developmental schedule of the postnatal rat testis determined by flow cytometry. *Biology of reproduction* 59, 84-92.
- Mikkelsen, T.S., Hanna, J., Zhang, X., Ku, M., Wernig, M., Schorderet, P., Bernstein, B.E., Jaenisch, R., Lander, E.S., and Meissner, A. (2008). Dissecting direct reprogramming through integrative genomic analysis. *Nature* 454, 49-55.
- Schultz, M.D., Schmitz, R.J., and Ecker, J.R. (2012). 'Leveling' the playing field for analyses of single-base resolution DNA methylomes. *Trends in genetics : TIG* 28, 583-585.
- Seisenberger, S., Andrews, S., Krueger, F., Arand, J., Walter, J., Santos, F., Popp, C., Thienpont, B., Dean, W., and Reik, W. (2012). The dynamics of genome-wide DNA methylation reprogramming in mouse primordial germ cells. *Molecular cell* 48, 849-862.